Zebrafish larvae as a powerful model to dissect protective innate immunity in response to *Legionella pneumophila* infection

Flávia Viana[1,§,#,*], Laurent Boucontet[2,§], Daniel Schator[1,3], Valerio Laghi[2], Marine Ibranosyan[4], Sophie Jarraud[4,5], Emma Colucci-Guyon[2,€,*] and Carmen Buchrieser[1,€,*]

[1]Institut Pasteur, Biologie des Bactéries Intracellulaires and CNRS UMR 3525, 75724, Paris, France, [2]Institut Pasteur, Unité Macrophages et Développement de l'Immunité and CNRS UMR 3738, Paris, France, [3]Sorbonne Université, Collège doctoral, 75005 Paris, France, [4]National Reference Centre of *Legionella*, Institute of Infectious Agents, Hospices Civils de Lyon, Lyon, France, [4] Hospices Civils de Lyon, Centre National de Référence des Legionella, Lyon, France, [5]Centre International de Recherche en Infectiologie, Université Lyon 1, UMR CNRS 5308, Inserm U1111, ENS de Lyon, Lyon, France

#Present Address: Wellcome-Wolfson Institute for Experimental Medicine, Queen's University Belfast, Belfast, United Kingdom

§ These authors contributed equally

€ Co-last authors

* Corresponding author's: cbuch@pasteur.fr, emma.colucci@pasteur.fr, f.d.m.viana@gmail.com

Key words: *Legionella pneumophila*, zebrafish, innate immune response; live imaging; neutrophils; macrophages

Lead contact:
Carmen Buchrieser
Institut Pasteur
Biologie des Bactéries Intracellulaires
28, rue du Dr. Roux,
75724 Paris Cedex 15, France
Tel: (33-1)-45-68-83-72
E-mail: *cbuch@pasteur.fr*

Abstract

The zebrafish has become a powerful model organism to study host-pathogen interactions. Here, we developed a zebrafish model of *Legionella pneumophila* infection to dissect innate immune responses. We show that *L. pneumophila* cause zebrafish larvae death in a dose dependent manner, and that macrophages are the first line of defence, with neutrophils cooperating to clear the infection. When either macrophages or neutrophils are depleted, the larvae become lethally sensitive to *L. pneumophila*. As observed in human infections, the adaptor signalling molecule Myd88 is not required to control disease in the larvae. Furthermore, proinflammatory cytokines IL-1β and TNFα were upregulated during infection, recapitulating key immune responses seen in human infection. We also uncovered a previously undescribed phenotype in zebrafish larvae, whereby bloodborne, wild type *L. pneumophila* invade and grow in the larval yolk region but not a T4SS mutant. Zebrafish larva represent an innovative *L. pneumophila* infection model closely mimicking important aspects of human infection.

.

INTRODUCTION

Legionella pneumophila, a gram negative, facultative intracellular bacterium inhabits natural, freshwater sources [1,2]. As an environmental, aquatic microbe *L. pneumophila* replicates intracellularly in aquatic protozoa [3]. Most interestingly, in contrast to other intracellular pathogens *L. pneumophila* is not adapted to a single host, but it exhibits a broad host range including Amoebozoa (amoebae), Percolozoa (excavates) and Ciliophora (ciliated protozoa) [3,4]. In the environment *L. pneumophila* can also be found within biofilms where it acquires nutrients from this mixed community, but it can also survive in a planktonic form for a certain time as well [5]. As fresh water and man-made systems are connected, *L. pneumophila* can also contaminate artificial water systems. Protected in its protozoan hosts *L. pneumophila* survives water disinfectants and may gain access to humans *via* aerosols produced by different man-made structures and devices. The inhalation of *L. pneumophila* contaminated aerosols can cause a severe pneumonia, the so-called Legionnaires' disease [6]. However, not every infection leads to disease. Disease outcome is determined by virulence of the bacterial strain, bacterial burden in the inhaled aerosols and most importantly by the host immune status. Host factors determining susceptibility include age above 50, smoking and/or having chronic lung disease, being immunocompromised and genetic factors that alter the immune response [2,7,8].

Once the bacteria reach the lungs of susceptible individuals, they can infect alveolar macrophages and replicate therein. After being phagocytosed *L. pneumophila* avoids lysosomes and establishes an endoplasmic reticulum derived vacuole named the *Legionella* containing vacuole (LCV) [9,10]. The LCV, a safe haven for bacterial replication, is established by utilizing the Dot/Icm type IV secretion system (T4SS) that injects over 350 proteins into the host cell [9-11]. These effector proteins manipulate a myriad of host pathways to recruit vesicles derived from the endoplasmic reticulum to the LCV, to supply the bacteria with nutrients, restrain autophagy and supress apoptosis or to subvert the host cell immune response [9-11]. A surprising high number of these effectors mimic host proteins and encode eukaryotic functions helping *L. pneumophila* to subvert numerous host pathways in remarkable diverse ways [11-13]

Intracellular bacterial replication and innate immune responses have been studied *in vitro* using both murine and human cell lines and *in vivo* using different animal models of *L. pneumophila* infection. However, results obtained with these models cannot be easily extrapolated to what is observed in human disease. Studies in invertebrate models, for example in *Galleria mellonella* and *Caenorhabditis elegans*, [14,15] require further validation in more developed models as their immune system greatly differs from that of vertebrates. More interestingly, mouse infection fails to recall the human disease phenotype, as most inbred mice strains are naturally resistant to *L. pneumophila* [16]. Very early after the discovery of *L. pneumophila* the guinea pig model of Legionnaires' disease was developed. Guinea pigs are highly susceptible to *L. pneumophila* when infected through injection into

the peritoneum [6] or when exposed to *L. pneumophila* containing aerosols [6]. Several studies thereafter have shown that the guinea pig infection model recalls human disease and allows to study the immune response to *L. pneumophila* infection [17,18]. However, the guinea pig model is now rarely used due to the limited availability of specific immunological reagents for these animals and the demanding laboratory and husbandry requirements to work with guinea pigs.

Since the above-mentioned models, including the widely used murine models, are limited for studying *L. pneumophila* infection *in vivo* and discrepancies exist between results obtained in mouse or human cells, the development of new, alternative models for *Legionella* infection is important. The zebrafish (*Danio rerio*) originally introduced as a model organism in developmental biology has emerged in recent years as a powerful non-mammalian model to study nearly every aspect of biology, including immune cell behaviour and host-pathogen interactions [19,20]. Zebrafish are evolutionary closer to humans than fruit flies and nematodes, easier to manipulate than mice and their immune system is remarkably similar to the one of mammals, making them an attractive laboratory model for immunology and infection biology [19,20]. Its popularity is also due to its small size and the natural translucency of its embryos and larvae, which makes it possible to follow leukocyte behaviour and infection onset at the level of the whole organism in real-time and high resolution [21]. Additionally, although adult organisms display a fully developed immune system with both active innate and adaptive branches, studies can also be conducted at the early stages of life (embryonic or larvae) when the organism solely relies on innate immunity, allowing to dissect the mechanisms arising from different immune responses [21-23]. Thus, we sought to examine whether the zebrafish could be an alternative model for analysing host-pathogen interactions and the innate immune response to *L. pneumophila* infection.

We show that *L. pneumophila* infection of zebrafish larvae recapitulate human disease onset, as infected wild-type larvae are generally able to clear the infection, but immunocompromised fish fail to do so. Both macrophages and neutrophils quickly interact and engulf injected *L. pneumophila*. Macrophage-depleted larvae show a dramatic increase of bacterial burden concomitant with host death, pointing to a crucial role of macrophages in controlling the infection. Interestingly, we discovered a new infection phenotype, as *L. pneumophila* replicates in the larvae yolk region, where it seems to be able to avoid the immune response of the host.

RESULTS

L. pneumophila infection induces mortality in zebrafish larvae in a dose dependent manner

To analyse whether *L. pneumophila* can cause disease in zebrafish larvae we microinjected larvae 72 hours post fertilisation (hpf) intravenously in the caudal vessels near the cloaca (UGO) (Fig 1A), with 10^3 or 10^4 CFU of wild type (WT) *L. pneumophila* strain Paris expressing GFP (WT-GFP) or the type IV

secretion system (T4SS) deficient isogenic mutant expressing GFP (Δ*dotA*-GFP). The infected larvae were kept at 28°C and were monitored regularly until 72 hours post infection (hpi) to record survival or death using a stereomicroscope. Larvae infected with doses of up to $3x10^3$ CFU of WT-GFP (defined as low dose, LD) all survived (100% survival). In contrast, larvae infected intravenously with doses of 10^4 CFU (defined as high dose, HD) resulted in approximately 30% of death within 72 hpi (Fig 1B). Importantly, all larvae injected with LD or HD of the Δ*dotA*-GFP strain survived for the entire time of observation (Fig 1B) indicating that the T4SS is important for replication in zebrafish larvae as it is in other infection models and in humans.

We then set up a method to monitor the bacterial burden of the infected zebrafish larvae. The progression of the infection was followed by analysing the bacterial load at 0, 24, 48 and 72 hpi comparing three different methods. First, we quantified the pixel counts of GFP fluorescence of live larvae images (Fig. S1A), secondly, we analysed the number of GFP expressing bacteria present in lysed infected larvae by FACS (Fig. S1B) and thirdly we plated serial dilutions of homogenates of euthanized larvae on BCYE medium (Fig S1C). The results obtained with the three methods were comparable (Fig S1). We choose to routinely monitor the *L. pneumophila* load of zebrafish larvae by FACS. As shown in Fig. 1C, larvae injected with LD of WT-GFP progressively eliminate the bacteria, by 24 hpi. Similarly, with high doses of Δ*dotA*-GFP were progressively cleared by 24 hpi. In contrast, some zebrafish larvae injected with HD of WT-GFP were unable to eliminate the bacteria at 72hpi, and the bacterial burden even increased by 48-72 hpi (Fig 1C). We also monitored infected larvae by fluorescent microscopy. Immediately upon injection (20 min to 2 hpi), bacteria were detectable as small foci, probably associated with professional phagocytes (Fig. 1D). By 24 hpi, in both, larvae injected with LD of WT-GFP as well as larvae injected with HD of the avirulent Δ*dotA*-GFP strain, the GFP signal declined becoming undetectable by 48 hpi, suggesting that the bacteria were progressively cleared. Despite showing the same pattern 24 hpi, larvae injected with HD of WT-GFP displayed a radically different progression of infection at 48 hpi, as bacterial proliferation started in a fraction of the infected larvae as seen by an increase in GFP signal. Most interestingly, in these larvae, bacterial proliferation occurred mainly in the yolk region while the bacterial load in the body decreased simultaneously. These bacterial foci in the yolk increased dramatically over time, causing death of the infected larvae by 72 hpi (Fig 1D).

Collectively our results indicate that *L. pneumophila* WT, but not the T4SS mutant induces death of zebrafish larvae. Larvae that were unable to control infection by 72 hpi, showed a unique phenotype, an increase of the bacterial burden in the yolk region.

Bloodstream L. pneumophila establishes a proliferative niche in the yolk region causing a persistent infection

To characterise the *L. pneumophila* foci identified in the yolk region of zebrafish larvae, we used high resolution fluorescent microscopy of HD of WT-GFP bloodstream injected in 72hpf Tg*(mfap4::mCherryF*) (herein referred as *mfap4*:mCherryF) (red macrophages) or Tg(*Lyz::DsRed)*^{nz50} (herein referred as *lyz*:DsRed)(red neutrophils) or Tg(*kdrl*::mCherry)^{is5} (red blood vessels) larvae. Upon injection of HD of WT-GFP, bacteria were progressively eliminated by the rest of the body and appeared growing in the yolk region between 48 and 72hpi, with macrophages accumulating there (Fig. 2A). We observed that *L. pneumophila* foci in the yolk region are highly complex, aggregate-like structures of long, filamentous bacteria growing in the yolk cell region and not in the visceral organs of the zebrafish larva. Macrophages were recruited to the yolk region containing *L. pneumophila,* (Fig. 2B, D Movie S1). Similarly, upon injection of HD of WT-GFP in *lyz*:DsRed larvae (red neutrophils), neutrophils were recruited to and accumulated around the growing bacterial aggregates, but seem unable to engulf them (Fig 2E, Movie S2).Moreover, confocal microscopy revealed that *L. pneumophila* exhibits grow in aggregates, and that these growing complex bacterial structures localize in the yolk and or in the yolk tube (Fig. 2F, Movie S3). Upon injection HD of WT-GFP in Tg(*kdrl*::mCherry)^{is5} (red blood vessels) larvae, we also showed that, the fast growing bacterial aggregates interact with the blood vessels (Fig 2G, Movie S4). It should be noted that the yolk is the only food source of the larvae during this developmental stage. The fast proliferation of the bacteria in the yolk region probably depletes its nutritional content, leading to larvae death (Fig 2, Movie S1). Strikingly, zebrafish larvae infected with the T4SS deficient Δ*dotA* mutant strain, did neither develop bacterial colonisation of the yolk nor larval death. This outcome was independent of the used dose, suggesting that zebrafish susceptibility to *L. pneumophila* infection and yolk penetration depends on a functional T4SS system.

Thus, blood-borne *L. pneumophila* is able to invade the yolk sac of zebrafish larvae, a previously undescribed phenotype of bacterial infection in this model. Once in the yolk, the bacteria replicate extensively, forming complex, organized, aggregate-like structures that cannot be removed by macrophages and neutrophils, thereby avoiding he host's immune control and clearance, eventually leading to death of the larvae.

Infection of zebrafish larvae with high doses of L. pneumophila leads to macrophage and neutrophil death

In human infection, alveolar macrophages are the primary cell type infected by *L. pneumophila* supporting its intracellular replication. Following infection, neutrophils are recruited to the lung and are key players for controlling infection as they possess antimicrobial activity and kill *L. pneumophila*

[24]. To analyse whether zebrafish infection mirrors human infection we monitored the interaction of zebrafish macrophages or neutrophils with the bacteria *in vivo*. The transgenic zebrafish larvae *mfap4*:mCherryF and *lyz*:DsRed were injected with low or high doses of WT-GFP or with high doses of Δ*dotA*-GFP. Infected larvae were monitored using widefield fluorescence microscopy and the number of leukocytes per larva was assessed by counting fluorescent macrophages and neutrophils over time until 72hpi. We observed that upon injection of high dose WT-GFP, the macrophage count decreased dramatically at 24hpi and then remained stable (Fig. 3A, B). Neutrophil counts gave similar results, as there was a dramatic decrease observed in neutrophil numbers starting at 24hpi, in particular after injection of high doses of WT bacteria Fig. 3C, D). Interestingly, upon infection with low doses of WT the neutrophil numbers decreased dramatically only at 24hpi but increased at 48hpi and 72hpi (Fig. 3D). In contrast macrophage and neutrophil counts remained unaffected upon injection of equal amounts of the avirulent Δ*dotA* strain, suggesting that phagocyte death is linked to a functional T4SS system.

Taken together, these results show that high dose *L. pneumophila* infection leads to a decrease in the number of professional phagocytes dependent on the T4SS, similar to what is seen during human infection by *L. pneumophila* and *Mycobacterium tuberculosis* [24,25]

Macrophages are the primary cells to phagocytise blood-borne L. pneumophila and neutrophils co-operate to decrease bacterial load

As macrophages and neutrophils are likely the phagocytes that interact with *L. pneumophila* we analysed phagocyte-*L. pneumophila* interactions *in vivo* by injecting *mfap4*:mCherryF or *lyz*:DsRed 72hpf larvae with WT-GFP or Δ*dotA*-GFP and recorded phagocyte-*L. pneumophila* interactions using high resolution confocal microscopy. This showed that upon injection of LD WT-GFP, macrophages immediately contacted and engulfed blood-borne bacteria, and the initial bacterial load was thereby unchanged for 8hpi. The GFP signal of the engulfed bacteria was present for a long time in macrophages, suggesting that live bacteria persist in macrophages *in vivo* over a certain period of time. However, macrophages were continuously recruited to the site of infection and by 16hpi the bacteria were mostly undetectable (Fig. 4A top panel, Movie S5). Macrophages that had engulfed a large amount of *L. pneumophila* stopped moving and rounded-up, suggesting cell death. Similarly, the inhibition of the migration of phagocytes by *L. pneumophila* has been observed previously during infection of RAW 264.7 macrophages and the amoeba *Dictyostelium discoideum* and *Acanthamoeba castellanii*, [26,27]. In contrast, zebrafish infected with HD of WT-GFP were not able to restrict the bacterial growth by 16hpi. HD of *L pneumophila* formed big aggregates, that were not easily engulfed and cleared by macrophages (Fig 4A, bottom panel, Movie S5). Remarkably, macrophages were very efficient in engulfing and rapidly clearing high doses of blood-borne Δ*dotA*-GFP bacteria. By 10hpi

most of the bacteria had been engulfed and cleared as suggested by the diffuse GFP staining in phagocytes (Fig. 4A, bottom panel, Movie S5). However, upon infection with a HD WT-GFP, bacteria were not completely cleared but persisted, and at 72hpi *L. pneumophila* was found in macrophages, suggesting that the bacteria are also replicating in macrophages of zebrafish larvae. Indeed, high resolution confocal microscopy showed that at 72hpi, *L. pneumophila* can also be found inside of macrophages in replicative vacuoles (Fig. S2).

The analyses of *L. pneumophila*-neutrophil interactions showed that these engulfed the bacteria trapped in the mesenchyme around the site of injection, but they were less efficient at clearing blood-borne bacteria. This is similar to what has been previously observed for infection of zebrafish larvae with *Escherichia coli* or *Shigella flexneri* [22,28]. Indeed, upon infection with a high dose of WT-GFP, *L. pneumophila* persisted in neutrophils and massive death of infected neutrophils occurred (Fig. 4B, second panel, Movies S6). In sharp contrast, neutrophils very efficiently engulfed and cleared large amounts of Δ*dotA*-GFP aggregated and trapped in the mesenchyme (Fig. 4B, lower panel, Movie S6) as well as low doses of WT-GFP (Fig 4B upper panel, Movie S6).

Altogether this shows that upon bloodstream injection of *L. pneumophila*, macrophages and neutrophils efficiently cooperate to eliminate the majority of bacteria within 20-24 hpi, with macrophages playing the primary role. However, *L. pneumophila* is also able to persist and replicate in macrophages. In contrast, neutrophils interact with *L. pneumophila* by quickly engulfing bacteria trapped in the mesenchyme near the site of injection but are less efficient in clearing blood-borne bacteria.

Macrophages are the first line defence restricting L. pneumophila infection

In humans, innate immune responses, based essentially on the activities of professional phagocytes and pro-inflammatory cytokine induction, are the key players to control and restrict *L. pneumophila* proliferation. Thus, human disease develops primarily in immunocompromised individuals [10]. To investigate whether the phagocytes of the innate immune system, macrophages and neutrophils, are also responsible for controlling *L. pneumophila* infection in zebrafish larvae, we selectively and transiently depleted macrophages or neutrophils, respectively and infected these "immunocompromised" larvae with *L. pneumophila*. Depletion of macrophages was achieved by knocking down the expression of s*pi1b*, a transcription factor involved in early myeloid progenitor formation. A low dose of s*pi1b* morpholino was reported to impact macrophages without affecting neutrophils [29]. We monitored the effect of low doses s*pi1b* morpholino injection on macrophage and neutrophil populations in double transgenic larvae with green neutrophils (*mpx*:GFP) and red

macrophages (*mfap4*:mCherryF). The specific depletion of the two cell types was confirmed by counting macrophages and neutrophils 72hpf (Fig S3A).

We then infected macrophage depleted larvae (s*pi1b* knockdown) by intravenous injection of LD or HD of WT-GFP. Independently of the infection dose, a dramatic decrease in survival occurred, as even injection of low doses of WT-GFP resulted in the death of 30% of the larvae (Fig 5A). When injecting high doses of WT-GFP nearly all of the infected larvae died by 72hpi, with the earliest deaths starting 48hpi (Fig 5A). In contrast, s*pi1b* knockdown larvae injected with high doses of Δ*dotA*-GFP did not show impaired survival (Fig 5A). The increased mortality correlated with an increased bacterial burden in s*pi1b* knockdown larvae compared to control larvae as judged from counting bacteria growing on BCYE agar from homogenates of individual larvae by FACS analyses (Fig 5B). Intravital imaging of infected s*pi1b* knock down larvae also showed that both low and high doses of WT-GFP failed to be cleared and that the bacteria established a replicative niche in the yolk, where they proliferated extensively (Fig 5C). This highlights, that macrophages are critical to restrict the onset of infection and *L. pneumophila* proliferation *in vivo*. Furthermore, these results also suggest that neutrophils, which are not depleted in s*pi1b* knockdown larvae, fail to control *L. pneumophila* infection in the absence of macrophages.

We next analysed the role of neutrophils in controlling the infection. Neutrophil development was disrupted by knocking down the G-CSF/GCSFR pathway using *csf3R* morpholino, previously reported to decrease up to 70% of the neutrophils present [30-32]. We then monitored the efficiency of the *csf3R* morpholino knockdown in double transgenic larvae confirming that 75% of the neutrophil population was depleted, while macrophage numbers were only slightly decreased (Fig S3B). When HD Δ*dotA*-GFP was injected, neutrophil-depleted larvae survived, and the bacterial burden remained unchanged, similar to what we had observed in infections of macrophage-depleted larvae (Fig. 5D, E). However, when neutrophil-depleted larvae were injected with HD WT-GFP, larvae survival significantly decreased and bacterial burdens increased at 48hpi (Fig. 5D, E). Neutrophil-depleted fish larvae showed an intermediate phenotype, displaying less survival and higher bacterial burden than in WT infected control larvae (Fig. 1A) but more survival and lower bacterial burden than in macrophage-depleted larvae (Fig. 5D, E). Intravital imaging showed that csf3R knockdown larvae that were unable to control *L. pneumophila* infection showed bacterial proliferation in the yolk comparable to WT control larvae (Fig 5F).

These results show that both neutrophils and macrophages are required for restricting and controlling *L. pneumophila* infection in the zebrafish model, but macrophages play the key role. Although neutrophils contributed less to clear the bacteria upon bloodstream injection, neutrophils might impact the infection outcome through cytokine release that can modulate macrophage activity.

Key pro-inflammatory cytokines are induced upon L. pneumophila infection of zebrafish larvae

Proinflammatory cytokines produced by infected and bystander cells during *L. pneumophila* infection of humans and mice play crucial roles in orchestrating host defences to control infection [33,34]. Infected cells produce IL-1α and IL-1β through a mechanism involving MyD88-dependent translational bypass. In contrast, bystander cells produce IL-6, TNF-α and IL-12 in an IL-1 receptor (IL-1R) dependant way [33,35]. To determine the pro-inflammatory responses of zebrafish larvae during *L. pneumophila* infection, we analysed *il1b*, *tnfa*, and *ifng1/2* (orthologues of mammalian *Ifng*) gene expression levels over time by qRT-PCR on RNA isolated from individual infected larvae. We found that infection of zebrafish larvae with LD or HD of WT-GFP induced a rapid (by 6hpi) and robust induction of *il1b* and *tnfa* gene expression. In larvae injected with low doses of WT-GFP the expression levels started to decrease by 24hpi, and gradually became undetectable at 72hpi. In contrast, larvae injected with HD of WT-GFP, expression of *il1b* and *tnfa* did not decrease over time (Fig. S3A and B) and a significant induction of *ifng1* was observed at 48hpi (Fig. S3C) but not of *ifng2* (Fig. S3D). In parallel, we scored the bacterial burden of the infected larvae before pro-inflammatory cytokine measurement at each time point under the microscope, which consistently showed that larvae with increased *il1b* and *tnfa* induction had also high bacterial burdens in the yolk and were not controlling the infection. These pro-inflammatory responses were T4SS dependent, as zebrafish larvae infected with HD of Δ*dotA*-GFP did not show significant induction of transcription of *tnfa*, *il1b* and *ing1/2* (Fig. S3 A-D).

Collectively, these results reveal, that key pro-inflammatory cytokines known to orchestrate the host response during *L. pneumophila* infection in humans are also induced in zebrafish larvae, and that cytokine gene induction is sustained when uncontrolled *L. pneumophila* proliferation occurs.

The immune response of zebrafish larvae to L. pneumophila infection is independent of MyD88 signalling

In innate immunity, the myeloid differentiation factor 88 (MyD88) plays a pivotal role in immune cell activation through Toll-like receptors (TLRs). MyD88-deficient mice are highly susceptible to *L. pneumophila* infection [36-39], however this is not the case when human macrophages are depleted of MyD88 [40]. Therefore, we sought to analyse which role MyD88 plays in zebrafish larvae during *L. pneumophila* infection. We injected *myd88-/-* and control larvae with LD or HD of WT-GFP, or with HD of Δ*dotA*-GFP and monitored larvae survival and bacterial burden over time as described in Figure 1. Our results show that susceptibility to infection of *myd88*-/- larvae injected with HD of WT-GFP, was comparable to that of WT larvae (Fig. 6A). Similarly, both control and *myd88*-/- larvae injected with LD WT-GFP or with the avirulent Δ*dotA*-GFP bacteria did not develop an infection, and the

bacterial burden decreased over time indicating that bacteria were cleared (Fig. 6A, B). To determine if pro-inflammatory responses were affected in the absence of MyD88 signalling, we analysed *il1b* and *tnfa* gene expression levels over time in control and *myd88*-/- larvae. Our results showed that *il1b* and *tnfa* gene expression levels were comparable in control and *myd88*-/- infected larvae for all conditions tested (LD WT-GFP and HD Δ*dotA*-GFP (Fig 6C, D).

Taken together, our results suggest that MyD88 signalling is not required for the innate immune response against *L. pneumophila* infection in the zebrafish larvae, which recapitulates human infection. However, MyD88 signalling may also be functionally compensated by other immune signalling pathways.

***Legionella pneumophila* replication in the yolk of zebrafish larvae is T4SS dependent**

Interestingly, replication of *L. pneumophila* mainly took place in the yolk region of infected zebrafish larvae (Movie S1-4, Fig. 2), dependent on a functioning T4SS as Δ*dotA*-GFP failed be detected in the yolk. To investigate whether the secretion mutant would be able to grow in the yolk cell when reaching it, we injected LD and HD of WT-GFP or Δ*dotA*-GFP directly into the yolk cell cytoplasm of 72hpf *lys*:DsRed zebrafish larvae (Fig. S4A). WT-GFP replicated extensively in the yolk region with low and high dose infections leading to rapid bacterial proliferation followed by a marked increase of the bacterial burden and death of the larvae (Fig. 7A, B). Surprisingly, Δ*dotA*-GFP did not replicate in the yolk even when injected directly but persisted over 72hpi. This result suggests that T4SS system is not only crucial for crossing the yolk sac syncytium but that its effectors are also necessary to obtain nutrients from the environment to allow replication. To further analyze this hypothesis, we selected a mutant in the gene encoding a sphingosine-1 phosphate lyase, (WT, Δ*spl)* [41] as we reasoned that this enzyme might be implicated in degrading sphingolipids present in the yolk of zebrafish larvae and thereby might aid *L. pneumophila* to obtain nutrients. Injection of Δ*spl* in the yolk sac region, and analyses of larvae death as compared to WT or Δ*dotA* showed that survival of zebrafish larvae injected with the Δ*spl* was slightly higher than with WT injected larvae (Fig. S4B), suggesting that the T4SS effector *Lp*Spl might be implicated in nutrient acquisition in the yolk environment.

Interestingly, the first isolation of *L. pneumophila* was achieved by inoculating the yolk region of embryonated eggs probably due to the richness in nutrients provided by the yolk [6]. Later yolk sacs of embryonated hen's eggs were used to produce polyvalent antigens for the diagnosis of *L. pneumophila* [42]. Thus, we decided to analyse *L. pneumophila* WT and Δ*dotA* phenotypes in the yolk sac of embryonated chicken eggs (ECE). We inoculated ECE directly in the yolk region with WT and with the Δ*dotA* strain at a concentration of 9.2 $\log_{10}$ CFU/mL and 9.1 $\log_{10}$ CFU/mL, respectively and assessed mortality of the embryos daily. The total mortality during the 6-day observation period in WT-GFP infected eggs was significantly higher (88.9%) than in the Δ*dotA*-infected eggs (14.3%;

p=0.010) or PBS inoculated control eggs (28.6%; *p*=0.010 and *p*=0.021, respectively), which were not significantly different from each other (p=0.253) (Fig. S4C). The highest mortality was observed at 2 days post infection in WT inoculated eggs with 55.6% mortality *versus* 0% in Δ*dotA* or 28.6% mortality in PBS inoculated eggs. Quantification of *L. pneumophila* in the yolk sac region at the day of mortality or at day 6 post infection revealed that the number of bacteria in the yolk sac of WT-infected ECE, was significantly higher than that in the yolk sac of those infected with the Δ*dotA* strain (7.8 $\log_{10}$ CFU/mL and 5.9 $\log_{10}$ CFU/mL, respectively, p=0.0127) (Fig. S4D). Controls inoculated with PBS (n=2) showed no *L. pneumophila* growth. Thus, like in zebrafish larvae only the WT strain is able to replicate in the yolk region and of inducing mortality in the embryos, while the T4SS mutant strain persists but is not able to replicate and does not induce high embryo mortality. This result further supports the finding that the T4SS system is crucial for obtaining nutrients when lipids are the major energy source available.

We next monitored neutrophil behaviour in the yolk-injected *lyz*:DsRed larvae in which neutrophils are labelled red. This showed that replication of WT-GFP in the yolk coincides with neutrophil death (Fig. 7C and D). The yolk cell is a single large cell where leukocytes were described to be unable to enter [43], but interestingly, macrophages and neutrophils were highly recruited to the yolk of WT-GFP infected larvae (Figure 2B-E), suggesting that *L. pneumophila* is sensed by the immune system even when replicating in the yolk, and could induce neutrophil death “at distance”. It is likely neutrophils can partly counteract *L. pneumophila* growth in the yolk by degranulating “at distance”, as previously shown in a zebrafish notochord infection model using non-pathogenic *E. coli* [32].

Our results suggest that the *L. pneumophila* T4SS plays a crucial role for the bacteria to pass from the blood circulation into the yolk and that T4SS effectors play an important role to obtain nutrients for bacterial proliferation.

DISCUSSION

In this study, we developed a zebrafish larva infection model for *L. pneumophila* and have analysed host pathogen interactions and the innate immune response of the host. We have found that a successful infection of zebrafish larvae by *L. pneumophila* depends on the infection site, the infection dose, the T4SS Dot/Icm and the host innate immune response, in particular macrophages and neutrophils. Wild type zebrafish larvae are susceptible to infection in a dose dependent manner, as larvae infected with a highly concentrated bacterial inoculum displayed bacterial dissemination and replication, concomitant with host death. However, as only about 30% of the larvae displayed this phenotype, the innate host defence of the larvae against *L. pneumophila* infection is relatively efficient. Thus, similar to what is observed in *L. pneumophila* infection of immune competent

individuals, the development of Legionnaire's disease is determined not only by the infection dose but also by the capacity of the host immune system to quickly and efficiently respond to infection.

Only blood borne bacteria are able to proliferate and induce mortality in zebrafish larvae. Once in the blood circulation, bacteria are actively engulfed and eliminated by both macrophages and neutrophils. However, some bacteria resist intracellular killing and replicate extensively inside macrophages (Fig. S2), get released into the blood flow and circulate in the zebrafish larvae. Some reach the yolk sac syncytium and T4SS competent *L. pneumophila* are able to cross this barrier and enter the yolk sac region. Once in the yolk, *L. pneumophila* gains a significant advantage in the pathogen-host arms race and establishes a replicative niche where it proliferates extensively. Indeed, in the yolk sac region *L. pneumophila* is protected from the host immune system as professional phagocytes are unable to enter in the yolk. Proliferation of the bacteria leads to host death, likely due to exhaustion of the nutrients present in the yolk, which are key in supporting the larvae development and due to the physical compression of the visceral developing organs, in particular the gastro-intestinal tract, exerted by the growing bacterial aggregate. Interestingly, we have also observed that in few cases the infected larvae were able to extrude the bacterial aggregates growing in the yolk and survived. This host defence mechanism has also been reported in a caudal fin model of *Mycobacterium marinum* infection, where infected zebrafish larvae extruded the bacteria-containing granuloma [44].

To our knowledge, the establishment of a replicative niche in the yolk upon injection in the bloodstream is unique to *L. pneumophila.* Most interestingly, direct yolk sac injection revealed that only the WT strain but not the T4SS knockout strain is able to replicate and establish a persistent infection, irrespective of the dose injected. This result points towards the involvement of the T4SS system and its secreted effectors in infection, replication and nutrient uptake in the yolk environment. Further analyses of this phenotype in embryonated chicken eggs, a commonly used model for antigen preparation, showed again, that only WT *L. pneumophila* are able to replicate in the yolk sac region, confirming the importance of the T4SS in nutrient uptake in addition to its known role in infection (Fig. S4A, B, C). *L. pneumophila* is known to mainly use amino acids as carbon and energy sources for growth [45] and secreted T4SS effectors have been shown to aid in amino acid uptake [46], however, fatty acids, glucose and/or glycerol also serve as carbon sources during the later stages of the life cycle of *L. pneumophila* [47,48], but no effectors connected to the uptake of these nutrients have been identified yet. The yolk cell is composed of a complex and dynamic mixture of different lipids on which the zebrafish larvae rely on for nutrition throughout development in the early larva phase. Cholesterol and phosphatidylcholine are the main constituents until 120hpf, with triacylglycerol, phosphatidylinositol, phosphatidylethanolamine, diacyl-glycerol, cholesteryl esters and sphingomyelins also present in significant concentrations [49]. *L. pneumophila* is known to secrete

437 several effectors with lipolytic activity through its T4SS which could be important for growth in a lipid
438 rich environment like the yolk (Hiller et al., 2018). In a first attempt to identify one of these effectors
439 we analysed the growth of a *L. pneumophila* mutant in a gene encoding a sphingosine-1 phosphate
440 lyase (*Lp*Spl) [41] compared to the WT strain after direct injection in the zebrafish larvae yolk sac.
441 Indeed, a small difference in larvae mortality was observed for the Δ*spl* strain, suggesting that *Lp*Spl
442 is one of several effectors that might participate in nutrient acquisition from lipids (Fig. S4B).
443 However, further analyses are needed to identify all effectors implicated in this phenotype.
444 Studies of *Legionella* infection in humans, guinea pigs and mouse lungs have shown that
445 *L. pneumophila* interacts closely with neutrophils and mononuclear phagocytes [50,51]. Professional
446 phagocytes are the main replication niche for *L. pneumophila* with monocytes and macrophages, in
447 particular alveolar macrophages, representing the main cells for replication in the lungs [52-55]. *In vivo*
448 studies in mice have shown that upon lung infection with *L. pneumophila* neutrophils, cDCs,
449 monocytes, and monocyte-like cells are rapidly recruited to the infection site, but although all these
450 cells seem to engulf the bacteria, *L. pneumophila* appears to be able to translocate effectors only into
451 neutrophils and alveolar macrophages. In zebrafish macrophages appear during the first days of
452 development, followed by neutrophils a day later forming together an efficient immune system that
453 protects the developing fish [23,56-58]. Therefore, the zebrafish larva offers a unique possibility to
454 interrogate the role of innate immune responses to infection [21]. Indeed, macrophage depleted larvae
455 showed a dramatically increased susceptibility to *L. pneumophila* infection as nearly 100% of larvae
456 inoculated with HD of WT and 30% of larvae inoculated with LD of *L. pneumophila* died from the
457 infection. Hence, macrophages are the first line of infection control against *L. pneumophila* and are
458 essential for restricting and controlling blood-borne infections, similar to what was observed for
459 *Burkholderia cenocepacia or Staphylococcus aureus* infection [59,60]. In contrast, when neutrophils were
460 depleted, the innate immune response was impaired to a lesser extent, suggesting that neutrophils
461 are required to ensure an effective innate immune response and, that macrophages alone are not
462 able to contain high burdens of *L. pneumophila* infection (Fig. 5).
463 Human innate immune signalling relies strongly on activation of Toll-like receptors (TLRs) and
464 respective adaptor molecules, all of which are highly conserved in the zebrafish [61,62]. One of these
465 adaptors is MyD88, known as a central player in interleukin 1 receptor (IL-1R) and TLR signalling in
466 humans and mammalian models [63]. MyD88 signalling is crucial for mice to combat *L. pneumophila*
467 infection, as it triggers the early secretion of inflammatory cytokines, neutrophil recruitment, and the
468 host immune response to the infection. Consequently, mice that lack MyD88 are highly susceptible
469 to infection [35-38]. However, in MyD88 depleted human macrophages *L. pneumophila* replication is not
470 different to replication in WT cells [40] Here we show, that *L. pneumophila* infected *myd88-/-* zebrafish
471 larvae have the same replication phenotype as WT larvae. Thus, Myd88 signalling does not play a key

role or may be redundant in the control of the innate immune response to *L. pneumophila* in zebrafish larvae, indicating that zebrafish mirrors human infection better than the mouse model. In the mouse model infected macrophages are incapable of producing cytokines, such as tumor necrosis factor (TNF) and interleukin-12 (IL-12), which are necessary to control infection. In contrast, infection of zebrafish larvae with WT *L. pneumophila* induced a rapid (by 6hpi) and robust induction of *il1b* and *tnfa* gene expression. However, it is thought that IL-1 released initially by *L. pneumophila*-infected macrophages drives the production of critical cytokines by bystander cells [33]. Infection of zebrafish larvae with HD of WT *L. pneumophila* induced a rapid (by 6hpi) and robust induction of *il1b* and *tnfa* gene expression whereas WT LD infection leads only to a short induction of *Il1b* transcript levels at 6hpi before declining to CTRL levels at later time points, suggesting that a short boost of IL-1β is sufficient to control LD of *L. pneumophila*. However, for a high load of *L. pneumophila* even a high and long-term induction of IL-1β is not allowing to control the infection, suggesting that the self-regulation of the immune response may be abrogated leading to a constant activation of IL-1β expression. Moreover, gene expression analyses also confirms that Myd88 has no influence on the control of the infection, as no difference in the transcript levels of *il1b*, *tnfa, ifng1 or infg2* was observed further suggesting that activation of the IL1R and certain TLR pathways are not crucial for *L. pneumophila* clearance in zebrafish larvae. One may even hypothesise that IL-1β release could be beneficial for *L. pneumophila* replication, as it was shown that IL-1β also may indicate an activation of the metabolic state of the bystander cells as it was shown that IL-1β induces a shift towards more metabolically active cells and increased cellular glucose uptake [64], which could aid *L. pneumophila* replication.

In conclusion, we have set up a new infection model for *L. pneumophila* that mimics human infection better than the mouse model. The unique advantages of the zebrafish provide now exciting possibilities to further explore different aspects of the relationship between, *L. pneumophila* and its host: the dynamics of bacterial dissemination, the interactions of the bacteria with macrophages and neutrophils, as well as the host immune response by intravital imaging.

EXPERIMENTAL PROCEDURES

Ethics Statement. Animal experiments were performed according to European Union guidelines for handling of laboratory animals ((http://ec.europa.eu/environment/chemicals/lab_animals/home_en.htm) and were approved by the Institut Pasteur Animal Care and Use Committee. and the French Ministry of Research (APAFIS#31827). The inoculation of embryonated chicken eggs is a standard procedure in diagnostics for the multiplication and antigen production of *Legionella* and is not covered by the national law for animal experiments in France (Décret n° 2013-118 du 1er février 2013).

Zebrafish care and maintenance. Wild-type AB fish, initially obtained from the Zebrafish International Resource Center (Eugene, OR), Tg(*Lyz::DsRed)*[nz50] [65], Tg*(mfap4::mCherryF*) (ump6Tg) [32] Tg(mpx:GFP)[i114] [66] , Tg(kdrl::mCherry)[is5] [67] and *myd88*[*hu3568*] mutant line (obtained from the Hubrecht Laboratory and the Sanger Institute Zebrafish Mutation Resource) [68], were raised in our facility. Eggs were obtained by natural spawning, bleached according to standard protocols, and kept in Petri dishes containing Volvic source water and, from 24 hours post fertilization (hpf) onwards 0.003% 1-phenyl-2-thiourea (PTU) (Sigma-Aldrich) was added to prevent pigmentation. Embryos were reared at 28°C or 24°C according to the desired speed of development; infected larvae were kept at 28°C. Timings in the text refer to the developmental stage at the reference temperature of 28.5°C. Larvae were anesthetized with 200µg/ml tricaine (Sigma-Aldrich) during the injection procedure as well as during *in vivo* imaging and processing for bacterial burden evaluation or cytokine expression studies.

Bacterial strains and growth conditions. *Legionella pneumophila* strain Paris carrying the pNT28 plasmid encoding for green fluorescent protein (constitutive GFP) [69], wild-type (WT-GFP) or Δ*dotA*-GFP were plated from -80°C glycerol stocks on N-(2-acetamido)-2-aminoethanesulfonic acid (ACES)-buffered charcoal yeast-extract (BCYE) medium supplemented with 10 µg/ml of chloramphenicol and cultured for 3 days at 37°C. Suspensions were prepared by resuspending bacteria in sterile 1x Phosphate Buffered Saline (PBS) and adjusting the OD 600 according to the desired bacterial concentrations for injection.

Morpholino injections. Morpholino antisense oligonucleotides (Gene Tools LLC, Philomath, OR, USA) were injected at the one to two cell stage as described [70]A low dose (4ng) of spi1b (previously named pu1) translation blocking morpholino (GATATACTGATACTCCATTGGTGGT) [71] blocks macrophage development only, but can also block neutrophil development when it is injected at a higher dose (20ng in 2nl). The csf3r translation blocking morpholino (GAACTGGCGGATCTGTAAAGACAAA) (4ng) [30] was injected to block neutrophil development. Control morphants were injected with 4ng control morpholino, with no known target (GAAAGCATGGCATCTGGATCATCGA).

Zebrafish infections. The volume of injected suspension was deduced from the diameter of the drop obtained after mock microinjection, as described in [70]. Bacteria were recovered by centrifugation, washed, resuspended at the desired concentration in PBS. 72h post-fertilization (hpf) anesthetized zebrafish larvae were microinjected iv or in the yolk with 0.5-1nl of bacterial suspension at the desired dose (~10^3 bacteria/nl for Low Dose (LD) and ~10^4 bacteria/nl for High Dose (HD) as described [22,28]. Infected larvae were transferred into individual wells (containing 1ml of Volvic water +

0.003% PTU in 24-well culture plates), incubated at 28°C and regularly observed under a stereomicroscope.

Evaluation of the bacterial burden in infected larvae. Infected zebrafish larvae were collected at 0, 24, 48 and 72hpi and lysed for analysing the bacterial burden by FACS. Each larva was placed in a 1.5 ml Eppendorf tube and anesthetized with tricaine (200µg/ml), washed with 1ml of sterile water and placed in 150 µl of sterile water. Larvae were then homogenized using a pestle motor mixer (Argos). Each sample was transferred to an individual well of a 96 well plate, counted on a MACSQuant VYB FACS (Miltenyi Biotec) and data analysed using FlowJo version 7.6.5. For CFU enumeration, serial dilutions were plated on BCYE agar plates supplemented with Chloramphenicol and the *Legionella* Selective Supplement GVPN (Sigma). Plates were incubated for 4-5 days at 37°C and colonies with the appropriate morphology and colour were scored using the G-Box imaging system (Syngene) and colonies enumerated using the Gene Tools software (Syngene).

***Dissociation of zebrafish larvae for FACS analysis of macrophages*.** Three to five Tg*(mfap4::mCherryF*) larvae were pooled in single 1.5 ml Eppendorf tubes and anesthetized with tricaine. The supernatant was discarded, and the larvae were resuspended in 1ml of 1x trypsin-EDTA solution (SIGMA) and incubated in a dry heat block at 30°C for 10 - 20 min. Every 2 minutes, the suspensions were homogenised by pipetting, until full homogenisation was reached. $CaCl_2$ (final concentration of 2µM) and foetal bovine serum (final concentration of 10%) were added to each tube and samples were kept on ice. Lysates were filtered using 40 µm strainers, washed with 20 ml ice cold 1X PBS and centrifuged 5 min at 1500 g, 4°C. Remaining pellets were resuspended in 250 µl 1X PBS and analysed with a MACSQuant VYB FACS (Miltenyi Biotec).

Live imaging, image processing and analysis. Quantification of total neutrophils and/or macrophages on living transgenic reporter larvae was performed upon infection as previously described [28]. Briefly, bright field, DsRed and GFP images of whole living anesthetized larvae were taken using a Leica Macrofluo™ Z16 APOA (zoom 16:1) equipped with a Leica PlanApo 2.0X lens, and a Photometrics® CoolSNAP™ *HQ2* camera. Images were captured using Metavue software 7.5.6.0 (MDS Analytical Technologies). Then larvae were washed and transferred in a new 24 wells plate filled with 1ml of fresh water per well, incubated at 28°C and imaged again under the same conditions the day after. Pictures were analysed, and Tg(*lyzC::DsRed*) neutrophils or Tg(*mfap4::mCherryF*) macrophages manually counted using the ImageJ software (V 1.52a). Counts shown in figures are numbers of cells per image.

The bacterial burden was measured by counting the total number of pixels corresponding to the GFP channel (Metavue software 7.5.6.0). Briefly, images corresponding to the GFP channel were adjusted to a fixed threshold that allowed to abrogate the background of the autofluorescence of the yolk. The same threshold was used for all images of one experiment. Histogram in the Analyze menu was used to obtain the number of black and white pixels. As shown in figure S1A, number of white pixels corresponding to *L. pneumophila* are plotted using GraphPad Prism® software.

High resolution confocal live imaging of injected larvae was performed as previously described [72]. Briefly, injected larvae were positioned in lateral or ventral position in 35 mm glass-bottom-Dishes (Ibidi Cat#: 81158). Larvae were immobilized using a 1% low-melting-point agarose (Promega; Cat#: V2111) solution and covered with Volvic water containing tricaine. A Leica SP8 confocal microscope equipped with two PMT and Hybrid detector, a 20X IMM objective (HC PL APO CS2 20X/0.75), a X–Y motorized stage and with the LAS-X software was used to live image injected larvae. To generate images of the whole larvae, a mosaic of confocal z-stack of images was taken with the 20X objective using the Tile Scan tool of the LAS-X software and was stitched together using the Mosaic Merge tool of the LAS-X software. All samples were acquired using the same settings, allowing comparisons of independent experiments. After acquisition, larvae were washed and transferred in a new 24-well plate filled with 1 ml of fresh water per well, incubated at 28°C and imaged again under the same conditions over time. A Leica SPE inverted confocal microscope and a 40x oil immersion oil immersion objective (ACS APO 40 × 1.15 UV) was also used to live image larvae infected with *L. pneumophila* Δ*dotA*-GFP (Figure 4).

The 4D files generated by the time-lapse acquisitions were processed, cropped, analysed, and annotated using the LAS-X and LAS-AF Leica software. Acquired Z-stacks were projected using maximum intensity projection and exported as AVI files. Frames were captured from the AVI files and handled with Photoshop software to mount figures. AVI files were also cropped and annotated with ImageJ software. Files generated with the LAS-X software were also processed and analysed with the Imaris software version9.5 (Bitplane, OXFORD Instruments) for 3D reconstruction, surfacing and volume rendering.

qRT-PCR to measure gene expression of cytokine encoding genes . RNA was extracted from individual larvae using the RNeasy® Mini Kit (Qiagen). cDNA was obtained using M-MLV H- reverse-transcriptase (Promega) with a dT_{17} primer. Quantitative PCR was performed on an ABI7300 thermocycler (Applied Biosystems) using TakyonTM ROX SYBR® 2X MasterMix (Eurogentec) in a final volume of 10 µl. Primers used: *ef1a (housekeeping gene used for normalization):* GCTGATCGTTGGAGTCAACA and ACAGACTTGACCTCAGTGGT*; il1b*: GAGACAGACGGTGCTGTTTA and

GTAAGACGGCACTGAATCCA*; tnfa*: TTCACGCTCCATAAGACCCA and CAGAGTTGTATCCACCTGTTA*; ifng-1-1*: ACCAGCTGAATTCTAAGCCAA and TTTTCGCCTTGACTGAGTGAA; *ifng-2:* GAATCTTGAGGAAAGTG AGCA and TCGTTTTCCTTGATCGCCCA

Statistical analysis. Normal distributions were analysed with the Kolmogorov– Smirnov and the Shapiro–Wilk tests. To evaluate difference between means of normally distributed data (for neutrophil and macrophage numbers), an analysis of variance followed by Bonferroni's multiple comparison tests was used. For bacterial burdens (CFU/FACS counts), values were Log10 transformed. Values of FACS and CFU counts did not pass the normality test, data were analysed following the Mann-Whitney test. For cytokine expression and bacterial burdens, non-Gaussian data were analysed with the Kruskal– Wallis test followed by Dunn's multiple comparison test. $P < 0.05$ was considered statistically significant (symbols: **** $P < 0.0001$; ***$P < 0.001$; **$P < 0.01$; *$P < 0.05$). Survival data were plotted using the Kaplan–Meier estimator and log-rank (Mantel–Cox) tests were performed to assess differences between groups. Statistical analyses were performed using GraphPad Prism® software. Statistical analyses for *in ovo* experiments, were performed using GraphPrism version 7. Comparison of survival curves between different infection groups was carried out with the Log-rank (Mantel-Cox) test. Comparisons of the means of *L. pneumophila* CFU counts between groups were performed by the Mann–Whitney test. A p-value under 0.05 was considered statistically significant.

Inoculation and quantification of *L. pneumophila* strains in *in ovo* experiments. Fertilized chicken eggs purchased from a local producer (Saint-Maurice-sur-Dargoire, Rhône, France) were incubated at 35°C in an egg incubator (Maino, Italy) to maintain normal embryonic development. Eggs were pathogen and antibiotic free. On day 0, 23 embryonated chicken eggs (ECE) were inoculated at 8 days of embryonation (DOE) with either *L. pneumophila* WT (n=9), *L. pneumophila ΔdotA* (n=7) or sterile PBS as control (n=7). *L. pneumophila* concentration in WT and Δ*dotA* suspensions before ECE injection was quantified at 9.2 $\log_{10}$ CFU/mL and 9.1 $\log_{10}$ CFU/mL, respectively. *L. pneumophila* concentration in the yolk sac of ECE directly after injection were estimated, considering both the measured inoculum counts and the yolk sac volumes (median (interquartile range) [IQR] volume, 30 [28.7-31.2] mL), at 7.4 and 7.3 $\log_{10}$ CFU/mL in the WT and Δ*dotA* groups, respectively. Two-day cultures of Lpp-WT and Lpp-Δ*dotA* on BCYE at 36°C were suspended in PBS at a DO = 2.5 McFarland (9 $\log_{10}$ CFU/mL) and 0.5 mL of suspensions or PBS as negative control were inoculated in the yolk sac of ECE. After inoculation, ECE were candled every 24 hours to assess embryo viability until day-6 post infection. Embryos that died the day after inoculation (n=2, corresponding to one WT-infected and one *ΔdotA*-infected embryo) were discarded for *L. pneumophila* quantification as death was probably

644 due to bad inoculation. Dead embryos were stored at 4°C overnight prior to harvesting the yolk sacs.
645 Remaining live embryos at 6-days post injection were euthanized by refrigeration overnight and the
646 yolk sacs were collected. After measuring their volume, yolk sacs were crushed using gentleMACS™
647 Octo Dissociator (Miltenyi Biotec, Germany) and 100 µL of serial dilutions at 10^{-2}, 10^{-4} and 10^{-6} were
648 automatically plated using easySpiral® automatic plater (Interscience, France) in triplicates on BCYE
649 agar. *L. pneumophila* were quantified after 5 days-incubation using Scan® 1200 Automatic HD colony
650 counter (Interscience, France).
651
652 **Author contributions**
653 FV, LB, DS, VL, MI and ECG performed the experiments, FV, SJ, LB, ECG and CB designed the
654 experiments, FV, LB, ECG analyzed the experiments, VL performed IMARIS analysis of the raw
655 confocal high resolution acquisition data, FV, ECG and CB wrote the article, ECG and CB supervised
656 the work and acquired funds.
657
658 **Competing Interest**
659 The authors declare there are no competing interests.
660
661 **ACKNOWLEDGEMENTS**
662 We thank Pedro Escoll and Jean-Pierre Levraud for help and ideas in the initial set up of the project
663 and Tobias Sahr for critical reading and helpful discussions and Yohann Rolin and Noël Aimar for their
664 excellent care of the fish. Work in the CB laboratory is financed by the Institut Pasteur, the Fondation
665 pour la Recherche Médicale (FRM) grant N° EQU201903007847 and the grant n°ANR-10-LABX-62-
666 IBEID. Work in ECG group is financed by Institut Pasteur, CNRS, and ANR grant N° 17-CE15-0026.
667 Valerio Laghi is funded by ANR grant TIFAsomes. We wish to thank the fish facility (Yohann Rolin and
668 Noël Aimar) for their excellent care of the fish. The funders, other than the authors, did not play any
669 role in the study or in the preparation of the article or decision to publish.
670
671 **REFERENCES**
672 1 Fliermans, C. B. Ecology of Legionella: From Data to Knowledge with a Little Wisdom. *Microb Ecol*
673 **32**, 203-228 (1996).
674 2 Cunha, B. A., Burillo, A. & Bouza, E. Legionnaires' disease. *Lancet* **387**, 376-385,
675 doi:10.1016/S0140-6736(15)60078-2 (2016).
676 3 Rowbotham, T. J. Preliminary report on the pathogenicity of *Legionella pneumophila* for
677 freshwater and soil amoebae. *J Clin Pathol* **33**, 1179-1183 (1980).
678 4 Boamah, D. K., Zhou, G., Ensminger, A. W. & O'Connor, T. J. From Many Hosts, One Accidental
679 Pathogen: The Diverse Protozoan Hosts of *Legionella*. *Frontiers in cellular and infection*
680 *microbiology* **7**, 477, doi:10.3389/fcimb.2017.00477 (2017).

5 Mampel, J. *et al.* Planktonic replication is essential for biofilm formation by *Legionella pneumophila* in a complex medium under static and dynamic flow conditions. *Appl Environ Microbiol* **72**, 2885-2895, doi:10.1128/AEM.72.4.2885-2895.2006 (2006).

6 McDade, J. E. *et al.* Legionnaires' disease: isolation of a bacterium and demonstration of its role in other respiratory disease. *N Engl J Med* **297**, 1197-1203 (1977).

7 Lanternier, F. *et al.* Legionnaire's Disease in Compromised Hosts. *Infect Dis Clin North Am* **31**, 123-135, doi:10.1016/j.idc.2016.10.014 (2017).

8 Naujoks, J., Lippmann, J., Suttorp, N. & Opitz, B. Innate sensing and cell-autonomous resistance pathways in Legionella pneumophila infection. *Int J Med Microbiol* **308**, 161-167, doi:10.1016/j.ijmm.2017.10.004 (2018).

9 Isberg, R. R., O'Connor, T. J. & Heidtman, M. The *Legionella pneumophila* replication vacuole: making a cosy niche inside host cells. *Nat Rev Microbiol* **7**, 13-24, doi:nrmicro1967 [pii]10.1038/nrmicro1967 (2009).

10 Mondino, S. *et al.* Legionnaires' Disease: State of the Art Knowledge of Pathogenesis Mechanisms of Legionella. *Annu Rev Pathol* **15**, 439-466, doi:10.1146/annurev-pathmechdis-012419-032742 (2020).

11 Ensminger, A. W. *Legionella pneumophila*, armed to the hilt: justifying the largest arsenal of effectors in the bacterial world. *Curr Opin Microbiol* **29**, 74-80, doi:10.1016/j.mib.2015.11.002 (2016).

12 Cazalet, C. *et al.* Evidence in the *Legionella pneumophila* genome for exploitation of host cell functions and high genome plasticity. *Nat Genet* **36**, 1165-1173 (2004).

13 Mondino, S., Schmidt, S. & Buchrieser, C. Molecular Mimicry: a Paradigm of Host-Microbe Coevolution Illustrated by Legionella. *mBio* **11**, doi:10.1128/mBio.01201-20 (2020).

14 Brassinga, A. K. *et al. Caenorhabditis* is a metazoan host for *Legionella*. *Cell Microbiol* **12**, 343-361, doi:CMI1398 [pii]10.1111/j.1462-5822.2009.01398.x (2009).

15 Harding, C. R. *et al. Legionella pneumophila* pathogenesis in the *Galleria mellonella* infection model. *Infect Immun* **80**, 2780-2790, doi:10.1128/IAI.00510-12 (2012).

16 Brown, A. S., van Driel, I. R. & Hartland, E. L. Mouse Models of Legionnaires' Disease. *Curr Top Microbiol* **376**, 271-291, doi:10.1007/82_2013_349 (2014).

17 Breiman, R. F. & Horwitz, M. A. Guinea pigs sublethally infected with aerosolized *Legionella pneumophila* develop humoral and cell-mediated immune responses and are protected against lethal aerosol challenge. A model for studying host defense against lung infections caused by intracellular pathogens. *J Exp Med* **165**, 799-811 (1987).

18 Weeratna, R. *et al.* Human and guinea pig immune responses to Legionella pneumophila protein antigens OmpS and Hsp60. *Infect Immun* **62**, 3454-3462 (1994).

19 Masud, S., Torraca, V. & Meijer, A. H. Modeling Infectious Diseases in the Context of a Developing Immune System. *Curr Top Dev Biol* **124**, 277-329, doi:10.1016/bs.ctdb.2016.10.006 (2017).

20 Torraca, V. & Mostowy, S. Zebrafish Infection: From Pathogenesis to Cell Biology. *Trends in Cell Biology* **28**, 143-156, doi:10.1016/j.tcb.2017.10.002 (2018).

21 Gomes, M. C. & Mostowy, S. The Case for Modeling Human Infection in Zebrafish. *Trends in Microbiology* **28**, 10-18, doi:10.1016/j.tim.2019.08.005 (2020).

22 Colucci-Guyon, E., Tinevez, J. Y., Renshaw, S. A. & Herbomel, P. Strategies of professional phagocytes in vivo: unlike macrophages, neutrophils engulf only surface-associated microbes. *J Cell Sci* **124**, 3053-3059, doi:10.1242/jcs.082792 (2011).

23 Herbomel, P., Thisse, B. & Thisse, C. Ontogeny and behaviour of early macrophages in the zebrafish embryo. *Development* **126**, 3735-3745 (1999).

24 Liu, X. & Shin, S. Viewing *Legionella pneumophila* Pathogenesis through an Immunological Lens. *J Mol Biol* **431**, 4321-4344, doi:10.1016/j.jmb.2019.07.028 (2019).

25 Cohen, S. B. *et al.* Alveolar Macrophages Provide an Early *Mycobacterium tuberculosis* Niche and Initiate Dissemination. *Cell Host Microbe* **24**, 439-446 e434, doi:10.1016/j.chom.2018.08.001 (2018).

26 Mengue, L. *et al. Legionella pneumophila* decreases velocity of Acanthamoeba castellanii. *Exp Parasitol* **183**, 124-127, doi:10.1016/j.exppara.2017.07.013 (2017).

27 Simon, S., Wagner, M. A., Rothmeier, E., Muller-Taubenberger, A. & Hilbi, H. Icm/Dot-dependent inhibition of phagocyte migration by *Legionella* is antagonized by a translocated Ran GTPase activator. *Cell Microbiol* **16**, 977-992, doi:10.1111/cmi.12258 (2014).

28 Mostowy, S. *et al.* The zebrafish as a new model for the in vivo study of *Shigella flexneri* interaction with phagocytes and bacterial autophagy. *PLoS Pathog* **9**, e1003588, doi:10.1371/journal.ppat.1003588 (2013).

29 Su, F. *et al.* Differential regulation of primitive myelopoiesis in the zebrafish by Spi-1/Pu.1 and C/ebp1. *Zebrafish* **4**, 187-199, doi:10.1089/zeb.2007.0505 (2007).

30 Ellett, F., Pase, L., Hayman, J. W., Andrianopoulos, A. & Lieschke, G. J. mpeg1 promoter transgenes direct macrophage-lineage expression in zebrafish. *Blood* **117**, e49-56, doi:10.1182/blood-2010-10-314120 (2011).

31 Palha, N. *et al.* Real-time whole-body visualization of Chikungunya Virus infection and host interferon response in zebrafish. *PLoS Pathog* **9**, e1003619, doi:10.1371/journal.ppat.1003619 (2013).

32 Phan, Q. T. *et al.* Neutrophils use superoxide to control bacterial infection at a distance. *Plos Pathogens* **14**, doi:ARTN e100715710.1371/journal.ppat.1007157 (2018).

33 Copenhaver, A. M., Casson, C. N., Nguyen, H. T., Duda, M. M. & Shin, S. IL-1R signaling enables bystander cells to overcome bacterial blockade of host protein synthesis. *Proc Natl Acad Sci U S A* **112**, 7557-7562, doi:10.1073/pnas.1501289112 (2015).

34 Friedman, H., Yamamoto, Y. & Klein, T. W. *Legionella pneumophila* pathogenesis and immunity. *Semin Pediatr Infect Dis* **13**, 273-279, doi:10.1053/spid.2002.127206 (2002).

35 Asrat, S., de Jesus, D. A., Hempstead, A. D., Ramabhadran, V. & Isberg, R. R. Bacterial pathogen manipulation of host membrane trafficking. *Annu Rev Cell Dev Biol* **30**, 79-109, doi:10.1146/annurev-cellbio-100913-013439 (2014).

36 Archer, K. A., Alexopoulou, L., Flavell, R. A. & Roy, C. R. Multiple MyD88-dependent responses contribute to pulmonary clearance of Legionella pneumophila. *Cell Microbiol* **11**, 21-36, doi:CMI1234 [pii]10.1111/j.1462-5822.2008.01234.x (2009).

37 Archer, K. A. & Roy, C. R. MyD88-dependent responses involving toll-like receptor 2 are important for protection and clearance of Legionella pneumophila in a mouse model of Legionnaires' disease. *Infect Immun* **74**, 3325-3333, doi:74/6/3325 [pii]10.1128/IAI.02049-05 (2006).

38 Hawn, T. R., Smith, K. D., Aderem, A. & Skerrett, S. J. Myeloid differentiation primary response gene (88)- and toll-like receptor 2-deficient mice are susceptible to infection with aerosolized Legionella pneumophila. *J Infect Dis* **193**, 1693-1702, doi:10.1086/504525 (2006).

39 Sporri, R., Joller, N., Albers, U., Hilbi, H. & Oxenius, A. MyD88-dependent IFN-gamma production by NK cells is key for control of Legionella pneumophila infection. *J Immunol* **176**, 6162-6171, doi:176/10/6162 [pii] (2006).

40 Mallama, C. A., McCoy-Simandle, K. & Cianciotto, N. P. The Type II Secretion System of *Legionella pneumophila* Dampens the MyD88 and Toll-Like Receptor 2 Signaling Pathway in Infected Human Macrophages. *Infect Immun* **85**, doi:10.1128/IAI.00897-16 (2017).

41 Rolando, M. *et al. Legionella pneumophila* S1P-lyase targets host sphingolipid metabolism and restrains autophagy. *Proc Natl Acad Sci U S A* **113**, 1901-1906, doi:10.1073/pnas.1522067113 (2016).

42 Fallon, R. J. & Abraham, W. H. Polyvalent heat-killed antigen for the diagnosis of infection with *Legionella pneumophila*. *J Clin Pathol* **35**, 434-438, doi:10.1136/jcp.35.4.434 (1982).

43 Levraud, J. P. *et al.* Real-time observation of *Listeria monocytogenes*-phagocyte interactions in living zebrafish larvae. *Infect Immun* **77**, 3651-3660, doi:10.1128/IAI.00408-09 (2009).

44 Hosseini, R. *et al.* Efferocytosis and extrusion of leukocytes determine the progression of early mycobacterial pathogenesis. *J Cell Sci* **129**, 3385-3395, doi:10.1242/jcs.135194 (2016).

45 Tesh, M. J. & Miller, R. D. Amino acid requirements for *Legionella pneumophila* growth. *J Clin Microbiol* **13**, 865-869 (1981).

46 Fonseca, M. V. & Swanson, M. S. Nutrient salvaging and metabolism by the intracellular pathogen *Legionella pneumophila*. *Frontiers in cellular and infection microbiology* **4**, 12, doi:10.3389/fcimb.2014.00012 (2014).

47 Hauslein, I., Manske, C., Goebel, W., Eisenreich, W. & Hilbi, H. Pathway analysis using (13) C-glycerol and other carbon tracers reveals a bipartite metabolism of *Legionella pneumophila*. *Mol Microbiol* **100**, 229-246, doi:10.1111/mmi.13313 (2016).

48 Hauslein, I. *et al. Legionella pneumophila* CsrA regulates a metabolic switch from amino acid to glycerolipid metabolism. *Open Biol* **7**, doi:10.1098/rsob.170149 (2017).

49 Fraher, D. *et al.* Zebrafish Embryonic Lipidomic Analysis Reveals that the Yolk Cell Is Metabolically Active in Processing Lipid. *Cell Rep* **14**, 1317-1329, doi:10.1016/j.celrep.2016.01.016 (2016).

50 Brieland, J. *et al.* Replicative *Legionella pneumophila* lung infection in intratracheally inoculated A/J mice. A murine model of human Legionnaires' disease. *Am J Pathol* **145**, 1537-1546 (1994).

51 Glavin, F. L., Winn, W. C., Jr. & Craighead, J. E. Ultrastructure of lung in Legionnaires' disease. Observations of three biopsies done during the Vermont epidemic. *Ann Intern Med* **90**, 555-559, doi:10.7326/0003-4819-90-4-555 (1979).

52 Horwitz, M. A. Formation of a novel phagosome by the Legionnaires' disease bacterium (*Legionella pneumophila*) in human monocytes. *J Exp Med* **158**, 1319-1331 (1983).

53 Horwitz, M. A. & Silverstein, S. C. Legionnaires' disease bacterium (*Legionella pneumophila*) multiples intracellularly in human monocytes. *J Clin Invest* **66**, 441-450 (1980).

54 Jager, J. *et al.* Human lung tissue explants reveal novel interactions during *Legionella pneumophila* infections. *Infect Immun* **82**, 275-285, doi:10.1128/IAI.00703-13 (2014).

55 Copenhaver, A. M. *et al.* Alveolar macrophages and neutrophils are the primary reservoirs for *Legionella pneumophila* and mediate cytosolic surveillance of type IV secretion. *Infect Immun* **82**, 4325-4336, doi:10.1128/IAI.01891-14 (2014).

56 Bennett, C. M. *et al.* Myelopoiesis in the zebrafish, *Danio rerio*. *Blood* **98**, 643-651, doi:10.1182/blood.v98.3.643 (2001).

57 Le Guyader, D. *et al.* Origins and unconventional behavior of neutrophils in developing zebrafish. *Blood* **111**, 132-141, doi:10.1182/blood-2007-06-095398 (2008).

58 Willett, C. E., Cortes, A., Zuasti, A. & Zapata, A. G. Early hematopoiesis and developing lymphoid organs in the zebrafish. *Dev Dyn* **214**, 323-336, doi:10.1002/(SICI)1097-0177(199904)214:4<323::AID-AJA5>3.0.CO;2-3 (1999).

59 Mesureur, J. *et al.* Macrophages, but not neutrophils, are critical for proliferation of *Burkholderia cenocepacia* and ensuing host-damaging inflammation. *PLoS Pathog* **13**, e1006437, doi:10.1371/journal.ppat.1006437 (2017).

60 Prajsnar, T. K., Cunliffe, V. T., Foster, S. J. & Renshaw, S. A. A novel vertebrate model of *Staphylococcus aureus* infection reveals phagocyte-dependent resistance of zebrafish to non-host specialized pathogens. *Cell Microbiol* **10**, 2312-2325, doi:10.1111/j.1462-5822.2008.01213.x (2008).

61 Jault, C., Pichon, L. & Chluba, J. Toll-like receptor gene family and TIR-domain adapters in *Danio rerio*. *Mol Immunol* **40**, 759-771, doi:10.1016/j.molimm.2003.10.001 (2004).

62 Meijer, A. H. *et al.* Expression analysis of the Toll-like receptor and TIR domain adaptor families of zebrafish. *Mol Immunol* **40**, 773-783, doi:10.1016/j.molimm.2003.10.003 (2004).

63 Akira, S. & Takeda, K. Toll-like receptor signalling. *Nat Rev Immunol* **4**, 499-511, doi:10.1038/nri1391 (2004).

64 Wik, J. A. *et al.* Inflammatory activation of endothelial cells increases glycolysis and oxygen consumption despite inhibiting cell proliferation. *FEBS Open Bio* **11**, 1719-1730, doi:10.1002/2211-5463.13174 (2021).

65 Hall, C., Flores, M. V., Storm, T., Crosier, K. & Crosier, P. The zebrafish lysozyme C promoter drives myeloid-specific expression in transgenic fish. *Bmc Dev Biol* **7**, doi:Artn 4210.1186/1471-213x-7-42 (2007).

66 Renshaw, S. A. *et al.* A transgenic zebrafish model of neutrophilic inflammation. *Blood* **108**, 3976-3978, doi:10.1182/blood-2006-05-024075 (2006).

836 67 van Leeuwen, L. M. *et al.* A transgenic zebrafish model for the in vivo study of the blood and
837 choroid plexus brain barriers using claudin 5. *Biol Open* **7**, doi:10.1242/bio.030494 (2018).
838 68 van der Vaart, M., van Soest, J. J., Spaink, H. P. & Meijer, A. H. Functional analysis of a zebrafish
839 myd88 mutant identifies key transcriptional components of the innate immune system. *Dis Model*
840 *Mech* **6**, 841-854, doi:10.1242/dmm.010843 (2013).
841 69 Tiaden, A. *et al.* The *Legionella pneumophila* response regulator LqsR promotes host cell
842 interactions as an element of the virulence regulatory network controlled by RpoS and LetA. *Cell*
843 *Microbiol* **9**, 2903-2920, doi:CMI1005 [pii]10.1111/j.1462-5822.2007.01005.x (2007).
844 70 Levraud, J. P., Colucci-Guyon, E., Redd, M. J., Lutfalla, G. & Herbomel, P. In vivo analysis of
845 zebrafish innate immunity. *Methods Mol Biol* **415**, 337-363, doi:10.1007/978-1-59745-570-1_20
846 (2008).
847 71 Brannon, M. K. *et al. Pseudomonas aeruginosa* Type III secretion system interacts with phagocytes
848 to modulate systemic infection of zebrafish embryos. *Cell Microbiol* **11**, 755-768,
849 doi:10.1111/j.1462-5822.2009.01288.x (2009).
850 72 Colucci-Guyon, E. *et al.* Spatiotemporal analysis of mycolactone distribution i*n vivo* reveals partial
851 diffusion in the central nervous system. *PLoS Negl Trop Dis* **14**, e0008878,
852 doi:10.1371/journal.pntd.0008878 (2020).
853

854

FIGURES LEGENDS

Figure 1. Zebrafish larvae are susceptible to intravenous *L. pneumophila* infection in a dose dependend manner. **A)** Scheme of the experimental set up of bacterial infection using zebrafish. A 72hpf zebrafish larva is shown. Bacteria are injected in the bloodstream (iv) via the caudal vein (green arrow). **B)** Survival curves (established from three independent experiments) of zebrafish larvae injected with WT-GFP Low Dose (WT LD) (blue curve, n=60) or High Dose (HD) (red curve, n=60), or with Δ*dotA*-GFP Low Dose (Δ*dotA* LD) (green curve, n=12) or High Dose (Δ*dotA* HD) (green curve, n=36), and incubated at 28°C. Non-injected fish (CTRL, black curve; n= 24). Three independent experiments. **C**) Bacterial burden quantification by enumerating live bacteria in homogenates from individual larvae infected with WT-GFP Low Dose (blue symbols) or High Dose (red symbols), or with Δ*dotA*-GFP High Dose (green symbols) measured by FACS immediately after *L. pneumophila* injection and 24h, 48h and 72h post *L. pneumophila* injection. n=10 larvae for each condition. **D)** Representative images of *L. pneumophila* dissemination, determined by live imaging using a fluorescence stereomicroscope, of zebrafish AB larvae infected with a LD or a HD of WT-GFP, or a HD of Δ*dotA*-GFP. The same infected larvae were live imaged 4h, 24h, 48h, and 72h post injection of the different *L. pneumophila* strains. GFP fluorescence of the injected bacteria is shown.

Figure 2. Bloodstream *L. pneumophila* establish a proliferative niche in the yolk causing a persistent local infection. Characterization of the *L. pneumophila* foci growing in the yolk region of zebrafish larvae. Maximum intensity projection of confocal acquisition using high resolution fluorescent microscope. **A)** 72hpf *mfap4*: mCherry larva (red macrophages) injected in the bloodstream with HD of WT-GFP and followed over time with confocal fluorescent microscopy. **B)** Imaris 3D reconstruction and volume rendering of the *L. pneumophila* growth in the yolk of the same infected larva at 72hpi, shown laterally. Inset shows the maximum intensity projection of the *L. pneumophila* foci in the same larva mounted ventrally. **C)** Scheme of 72hpf larva indicating with green dots the yolk sustaining *L. pneumophila* growing. **D**) Imaris 3D reconstruction and volume rendering of the *L. pneumophila* growth (GFP labelling) in the yolk of the same infected larva at 72hpi, showed ventrally. **E)** Imaris 3D reconstruction and volume rendering of the *L. pneumophila* growth in the yolk of *lyz*:DsRed (red neutrophils) infected larva at 72hpi, showed laterally. **F)** Imaris 3D reconstruction and volume rendering of the *L. pneumophila* growth (GFP labelling) in the yolk of wild type AB infected larva at 72hpi, showed laterally. Overlay of GFP and mCherry, or DsRed fluorescence is shown (2B, E, G), and BF is shown to help to visualize the yolk region and host anatomy (2A, D, F). See also related Movies S1-S4.

Figure 3. *L. pneumophila* high dose infection results in (systemic) macrophage and neutrophil death. A) Representative images of *L. pneumophila* dissemination, determined by live imaging using a fluorescence stereomicroscope of zebrafish Tg*(mfap4::mCherryF)* larvae infected with a Low Dose or a HD of WT-GFP, or a HD of Δ*dotA*-GFP. The same infected larvae were live imaged 4h, 24h, 48h, and 72h post *L. pneumophila* injection. Overlay of GFP and mCherry fluorescence is shown. **B)** Macrophage counts in uninfected larvae (black symbols) or upon Low Dose (blue symbols) or High Dose of WT-GFP (red symbols), or High Dose (green symbols) of Δ*dotA* -GFP injections. Macrophages were counted manually from images taken on live infected larvae, using ImageJ software, and results were plotted using GraphPad Prism® software. Mean±SEM are also shown (horizontal bars). Data plotted are from two pooled independent experiments (n=12 larvae scored for each condition). **C)** Representative images of *L. pneumophila* dissemination, determined by live imaging using a fluorescence stereomicroscope, of zebrafish Tg(*LysC::DsRed)*^{nz50} larvae infected with a Low Dose or a High Dose of WT-GFP or a High Dose of Δ*dotA*-GFP. The same infected larvae were live imaged 4h, 24h, 48h, and 72h post *L. pneumophila* injection. Overlay of GFP and DsRed fluorescence is shown. **D)** Neutrophil counts in uninfected (CTRL, black symbols) or upon Low Dose or High Dose of WT-GFP (blue or red symbols), or High Dose of Δ*dotA*-GFP (green symbols) injections. Data plotted in the same way as for macrophage counts, are from two pooled independent experiments (n=10 larvae scored for each condition).

Figure 4. Live imaging of macrophage and neutrophil interaction with *L. pneumophila*

Frames extracted from maximum intensity projection of *in vivo* time-lapse confocal fluorescent microscopy of 72hpf Tg*(mfap4::mCherryF)* larvae injected in the bloodstream (iv) with a LD, HD (of WT-GFP or a HD of Δ*dotA*-GFP (upper panel) or Tg(*LysC::DsRed)*^{nz50} in the bloodstream (iv) with a LD, HD of WT-GFP or a HD of Δ*dotA*-GFP (lower panel) to follow macrophage and neutrophil interaction with *L. pneumophila* respectively. Images were taken from time lapse at different time points (0hpi, 2hpi, 4hpi, 8hpi and 16hpi). Overlay of green (*L. pneumophila*) and red (leucocytes) fluorescence of the caudal area of the larvae (region boxed in the scheme on the right of the panel) is shown. Scale bar: 50μm. See also related Movies S5, S6.

Figure 5. Macrophages are crucial to restrict *Legionella pneumophila* dissemination

A) Survival curves of CTRL morphant zebrafish larvae injected with a Low Dose (LD) (blue dashed curve, n=34 larvae) or a High Dose (HD) (red dashed curve, n=34) of WT-GFP, or with a HD (green dashed curve, n=24) of Δ*dotA* -GFP, and spi1b morphant zebrafish larvae injected with a LD (blue curve, n=48) or a HD (red curve, n=48) of WT-GFP, or with a High Dose (HD) (green curve, n=48) of Δ*dotA* -GFP. Non-injected CTRL morphant fish (black dashed curve, n=48), and spi1b morphant fish

(black curves, n=48) were used as control. Infected and control larvae were incubated at 28°C. Data plotted are from two pooled independent experiments. **B)** and **E**) Bacterial burden quantification by enumerating live bacteria in homogenates from individual larvae infected with LD of WT-GFP (blue symbols) or HD (red symbols), or with LD of Δ*dotA*-GFP (magneta symbols) or HD (green symbols), measured by plating onto BCYE agar plates supplemented with Chloramphenicol and the *Legionella* Selective Supplement GVPN immediately after *L. pneumophila* injection and 24h, 48h and 48h post *L. pneumophila* injection. n=10 larvae for each condition. **D)** Survival curves of CTRL morphant zebrafish larvae injected with a LD (blue dashed curve, n=36) or a HD (red dashed curve, n=36) of WT-GFP, or with a HD (green dashed curve, n=24) of Δ*dotA* -GFP, and csf3r morphant zebrafish larvae injected with a LD (blue curve, n=24) or a HD (red curve, n=36) of WT-GFP, or with a HD (green curve, n=36) of Δ*dotA* -GFP. Non-injected CTRL morphant fish (black dashed curve, n=48), and csf3r morphant fish (black curve, n=36) were used as control. Data plotted are from two pooled independent experiments. **C)** and **F)** Representative images of *L. pneumophila* dissemination, determined by live imaging using a fluorescence stereomicroscope, of Tg*(mfap4::mCherryF*) *spe1b* morphant larvae (**C**) and of Tg(*LysC::DsRed)*^{nz50} (**F)** csf3r morphant larvae non infected, or infected with a LD or a HD of WT-GFP, or a HD of Δ*dotA*-GFP. The same infected larvae were live imaged 4h, 24h, 48h, and 72h post *L. pneumophila* injection. Overlay of GFP and mCherry fluorescence is shown.

Figure 6. Zebrafish larva Immunity to *L. pneumophila* is independent from signalling through MyD88 or compensated by other signalling pathways. **A**) Survival curves of CTRL zebrafish larvae injected with WT-GFP Low Dose (LD) (blue dashed curve) or High Dose (HD) (red dashed curve), or with Δ*dotA* -GFP HD (green dashed curve), and *myd88*^{hu3568} mutant zebrafish larvae injected with WT-GFP LD (blue curve) or HD (red curve), or with Δ*dotA* -GFP HD (green curve). Non-injected CTRL larvae (black dashed curves), and *myd88*^{hu3568} mutant larvae (black curves) were used as control. Infected and control larvae (n= 72 fish for *myd88*^{hu3568} mutant conditions and n= 57 fish for CTRL conditions) were incubated at 28°C. Data plotted are from 3 pooled independent experiments. **B)** Bacterial Burden of *myd88*^{hu3568} mutant zebrafish larvae are the same as what is observed for control larvae. Bacterial burden quantification by enumerating live bacteria in homogenates from individual larvae infected with WT-GFP LD (blue symbols) or HD (red symbols), or with Δ*dotA* -GFP HD (green symbols) were measured by plating onto BCYE agar plates supplemented with Chloramphenicol and the *L. pneumophila* Selective Supplement GVPN immediately after *Legionella* injection and 24h, 48h and 48h post *Legionella* injection. n=15 larvae for each condition. **C-D)** Cytokine (*il1b*, *tnfa*) induction was measured from individual *myd88*^{hu3568} mutant larvae injected with a HD (red curves) of WT-GFP and non-injected fish as control (CTRL, black curves). The same colours are used in individual CTRL zebrafish with dashed curves. Data plotted are from one experiment (n=5 larvae for each condition);

individual values are shown, and curves correspond to the medians. There is no statistically significant difference between CTRL and *myd88*^{hu3568} mutant curves over time for all the conditions analysed.

Figure 7. *L. pneumophila* replication in the yolk of zebrafish larvae is T4SS dependent. **A)** Survival curves of zebrafish larvae injected with WT-GFP Low Dose (LD) (blue curve) or High Dose (HD) (red curve), or with Δ*dotA*-GFP LD (magenta curve) or HD (green curve). Non-injected larvae (black curves) were used as control. n= 48 larvae per conditions. All larvae were incubated at 28°C. Data plotted are from two pooled independent experiments. **B**) Bacterial burden quantification of zebrafish larvae injected with *L. pneumophila* in the yolk cell, by enumerating live bacteria in homogenates from individual larvae infected with WT-GFP LD (blue symbols) or HD (red symbols), or with Δ*dotA*-GFP Low Dose (LD) (magenta symbols) or HD (green symbols). They were measured by plating onto BCYE agar plates supplemented with Chloramphenicol and the *Legionella* Selective Supplement GVPN immediately after *L. pneumophila* injection and 24h, 48h and 48h post *Legionella* injection. n=10 larvae for each condition. **C-D**) Representative images of *L. pneumophila* dissemination, determined by live imaging using a fluorescence stereomicroscope, of Tg(*LysC::DsRed)*^{nz50} not infected zebrafish larvae, or infected with a Low Dose of WT-GFP or Δ*dotA* -GFP (C), or infected with a High Dose of WT-GFP or Δ*dotA* -GFP (D). The same infected larvae were live imaged 4h, 24h, 48h, and 72h post *L. pneumophila* injection. Overlay of GFP and mCherry fluorescence is shown.

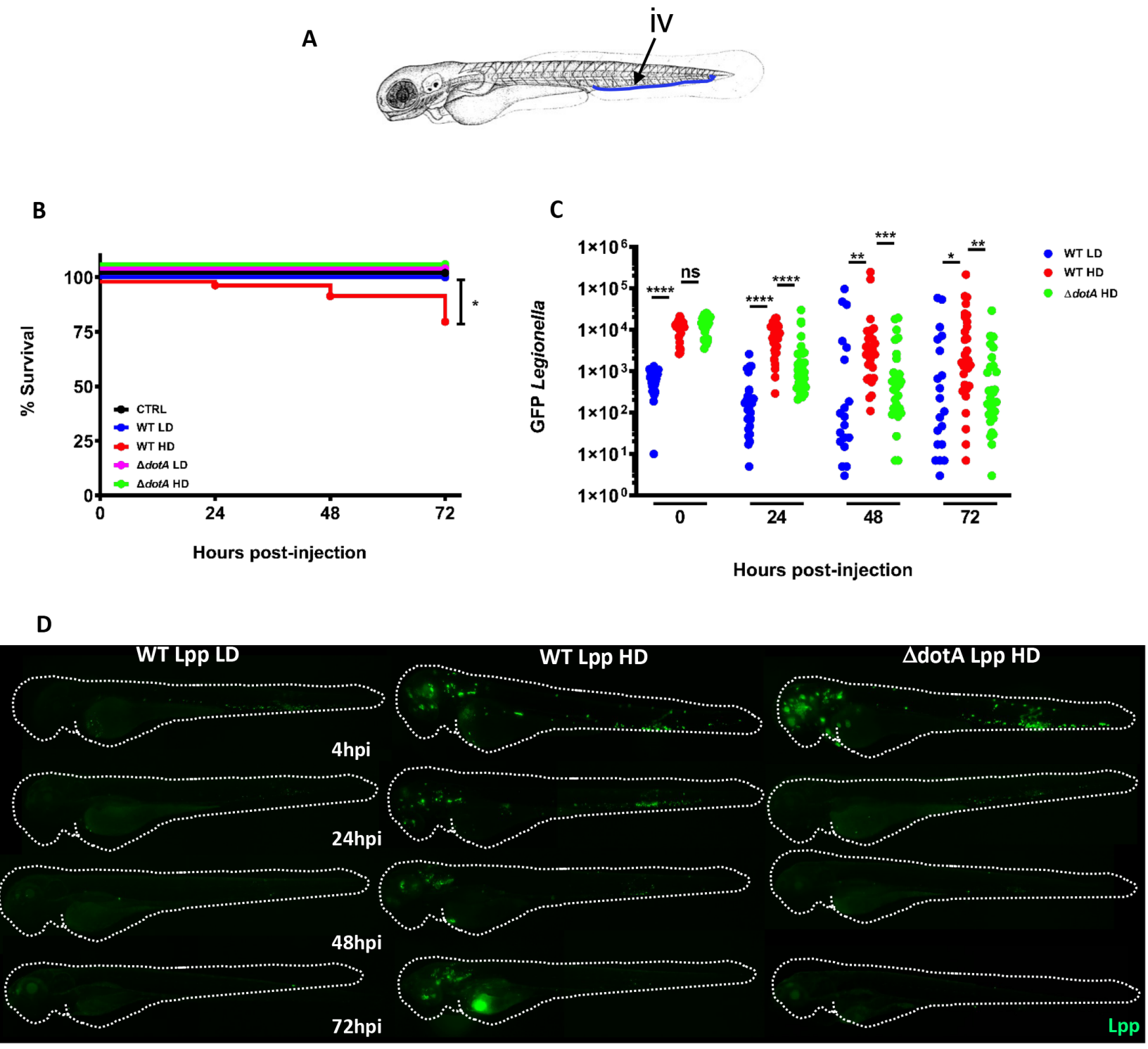
A
iv
B
% Survival
100
75
50
25
0
0
24
48
72
Hours post-injection
CTRL
WT LD
WT HD
ΔdotA LD
ΔdotA HD
*
C
GFP Legionella
1×10^6
1×10^5
1×10^4
1×10^3
1×10^2
1×10^1
1×10^0
ns
****
****
****
**
***
*
**
0
24
48
72
Hours post-injection
WT LD
WT HD
ΔdotA HD
D
WT Lpp LD
WT Lpp HD
ΔdotA Lpp HD
4hpi
24hpi
48hpi
72hpi
Lpp

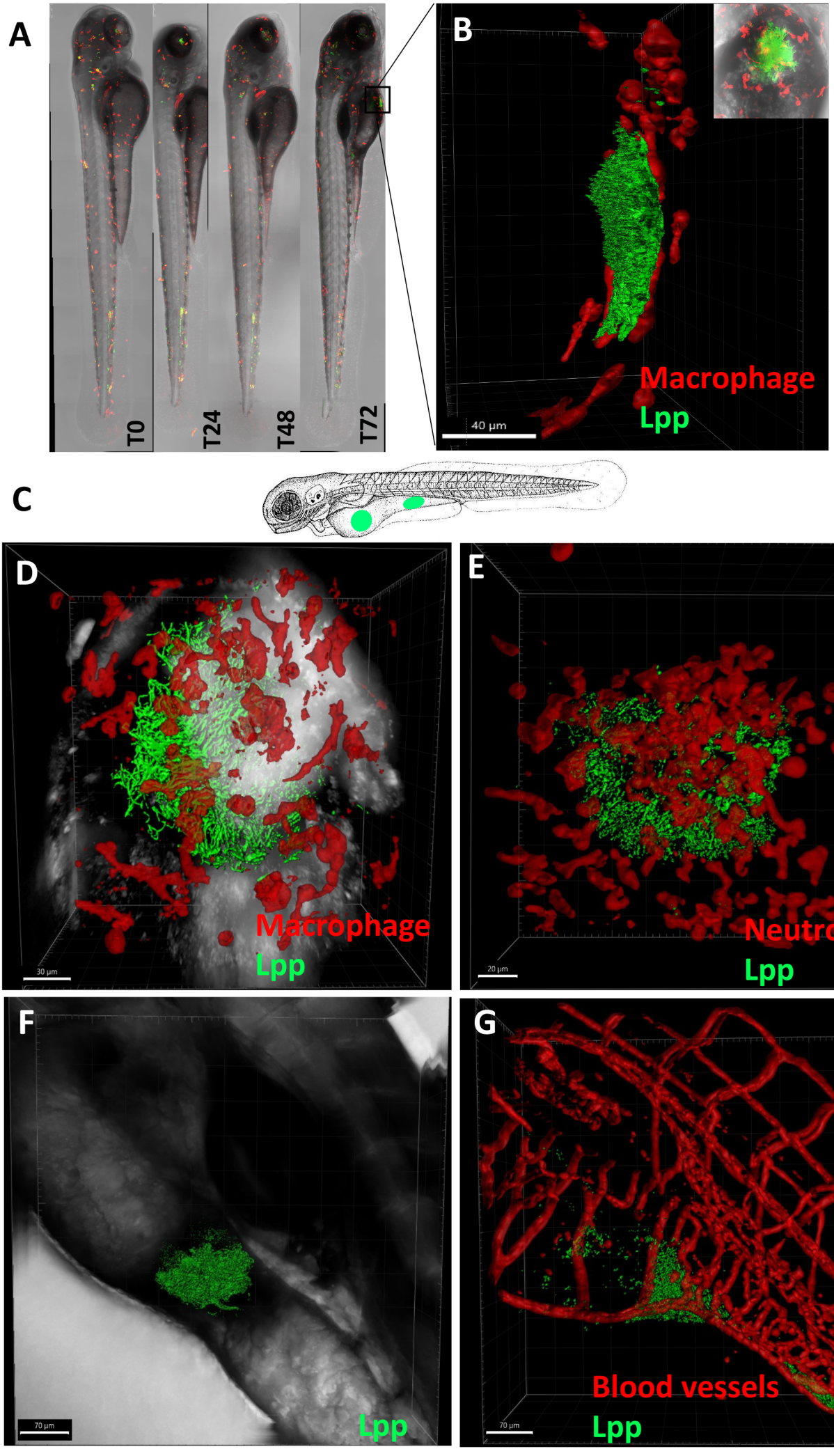
A
T0
T24
T48
T72
B
Macrophage
Lpp
40 µm
C
D
Macrophage
Lpp
30 µm
E
Neutrophil
Lpp
20 µm
F
Lpp
70 µm
G
Blood vessels
Lpp
70 µm

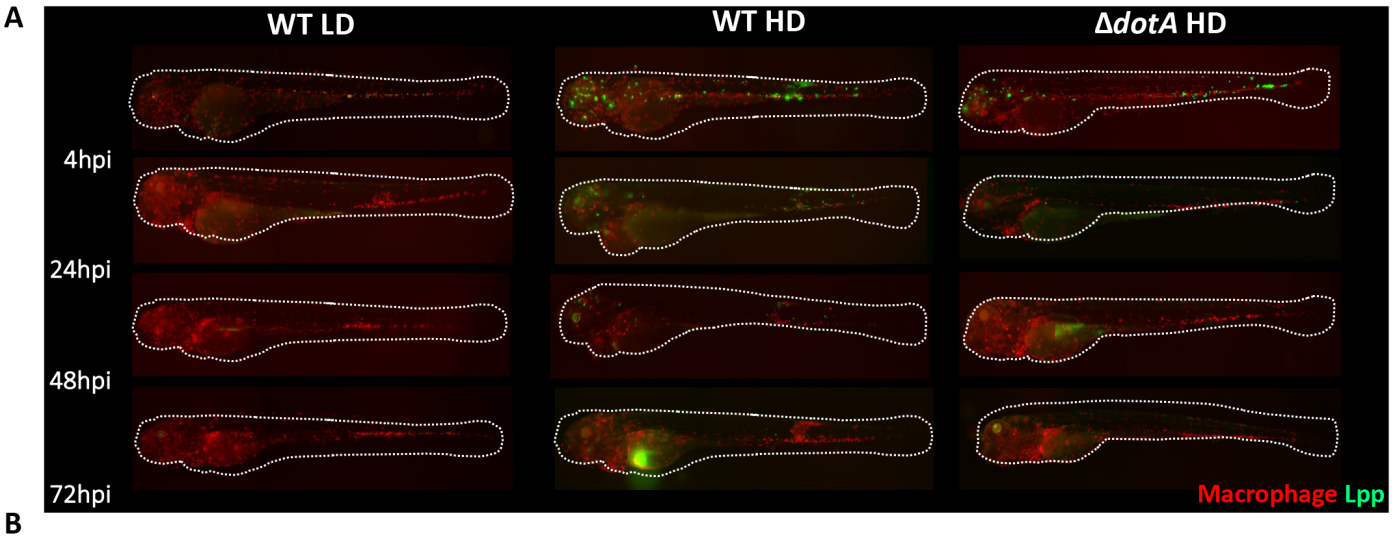
A
WT LD
WT HD
ΔdotA HD
4hpi
24hpi
48hpi
72hpi
Macrophage Lpp

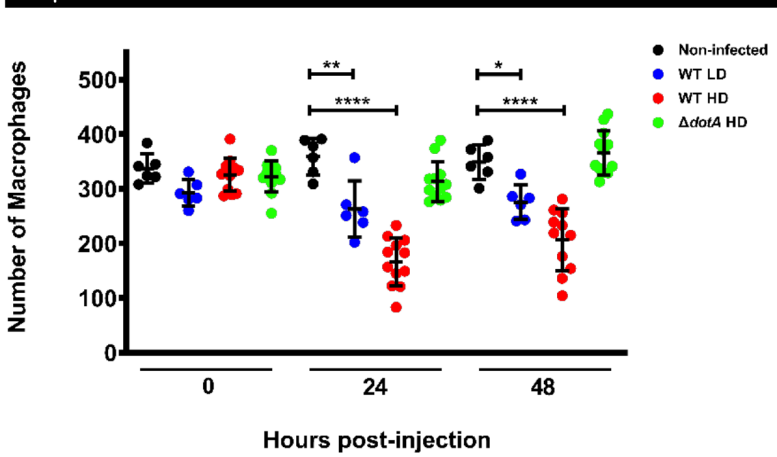
B
Number of Macrophages
500
400
300
200
100
0
**
****
*
****
0
24
48
Hours post-injection
Non-infected
WT LD
WT HD
ΔdotA HD

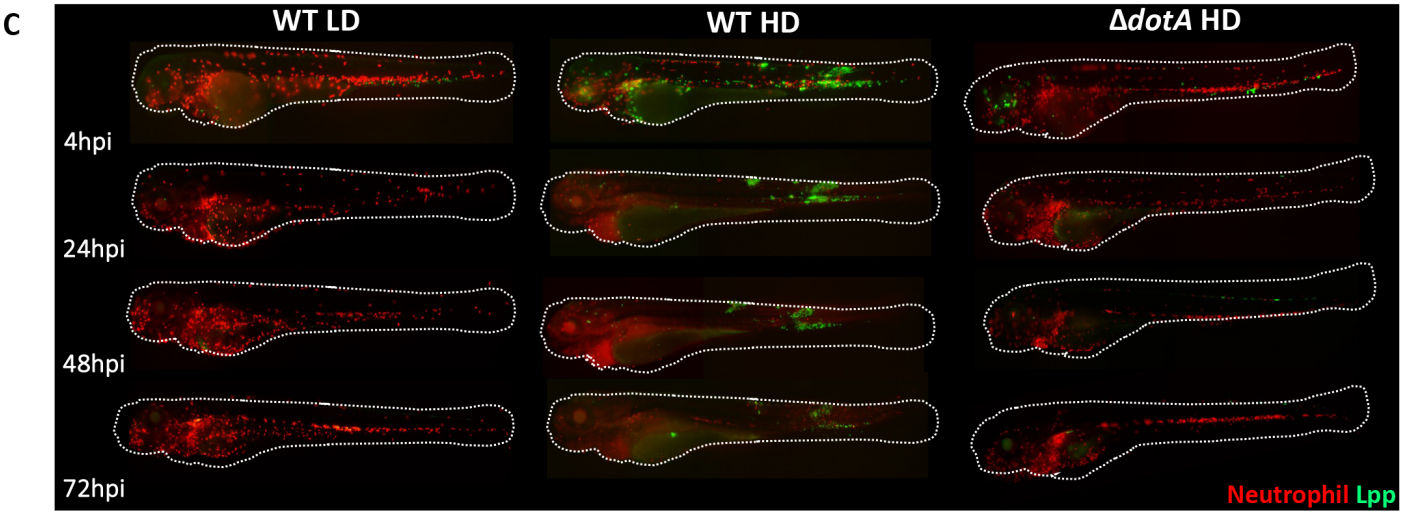
C
WT LD
WT HD
ΔdotA HD
4hpi
24hpi
48hpi
72hpi
Neutrophil Lpp

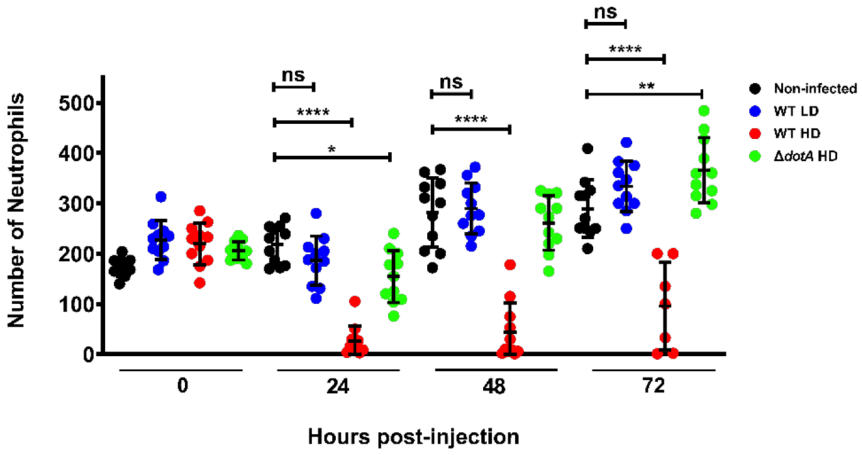
D
Number of Neutrophils
500
400
300
200
100
0
ns
****
*
ns
****
ns
****
**
0
24
48
72
Hours post-injection
Non-infected
WT LD
WT HD
ΔdotA HD

Macrophage-Lpp interactions over time

A

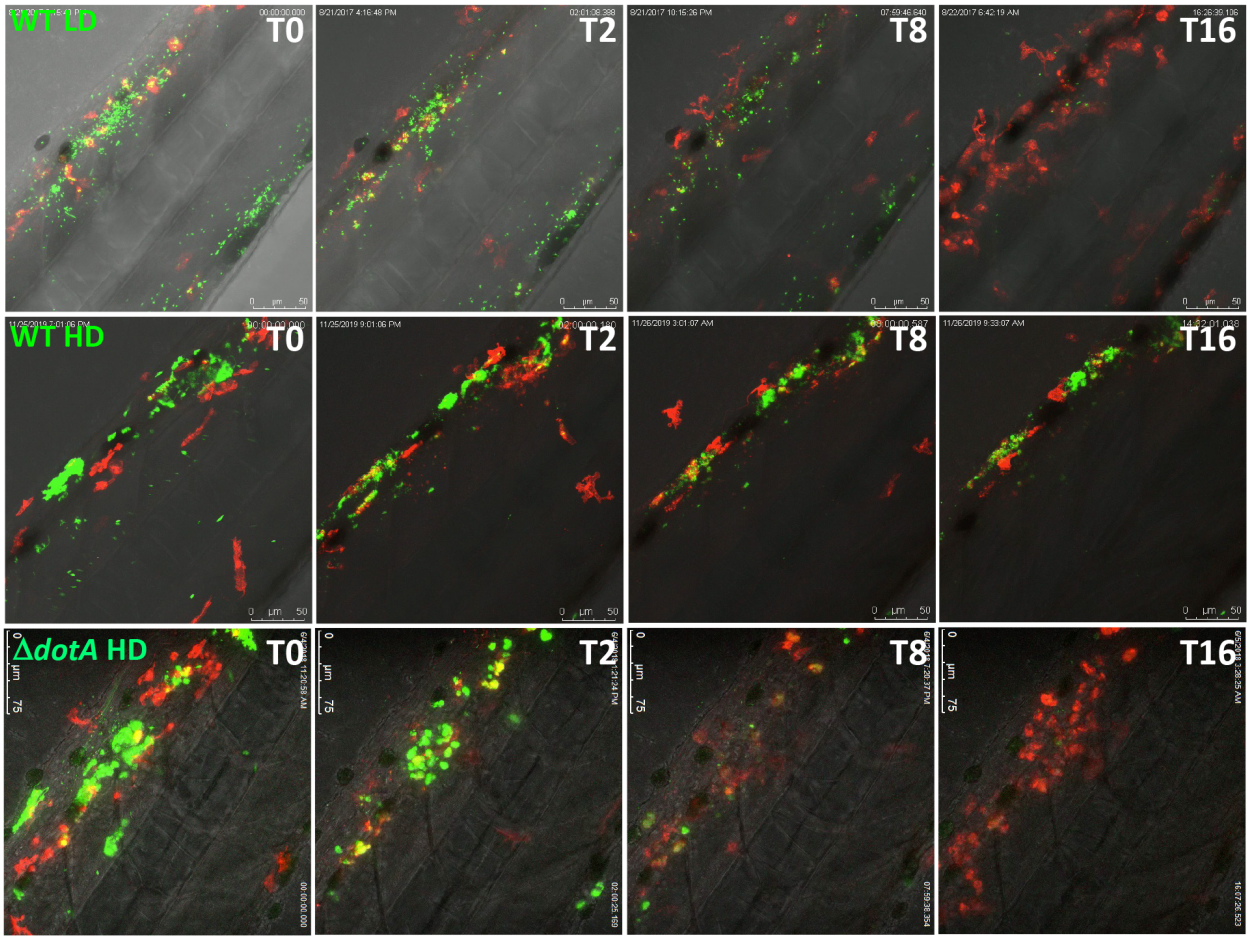

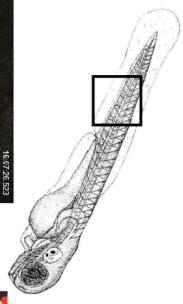

Neutrophil-Lpp interactions over time

B

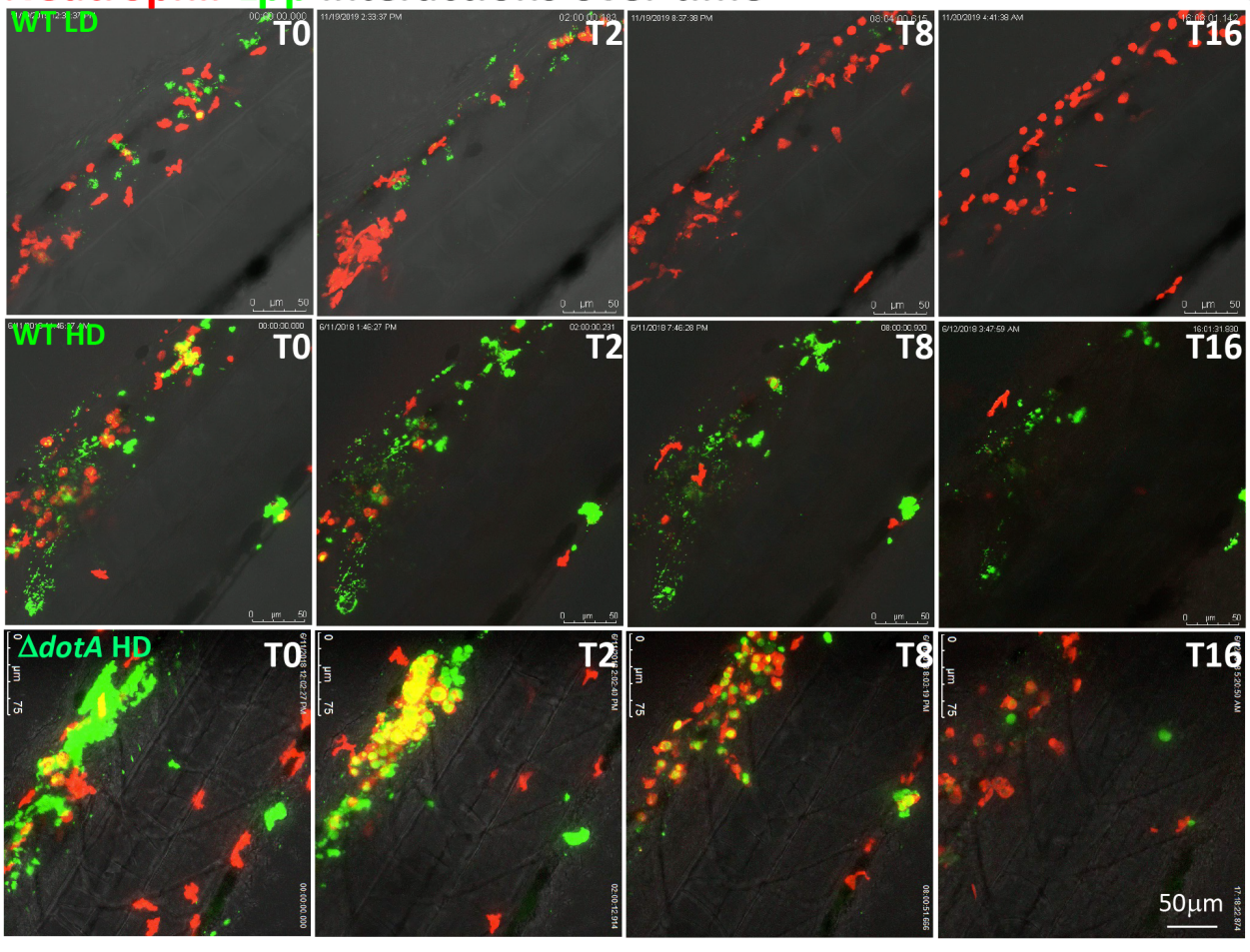

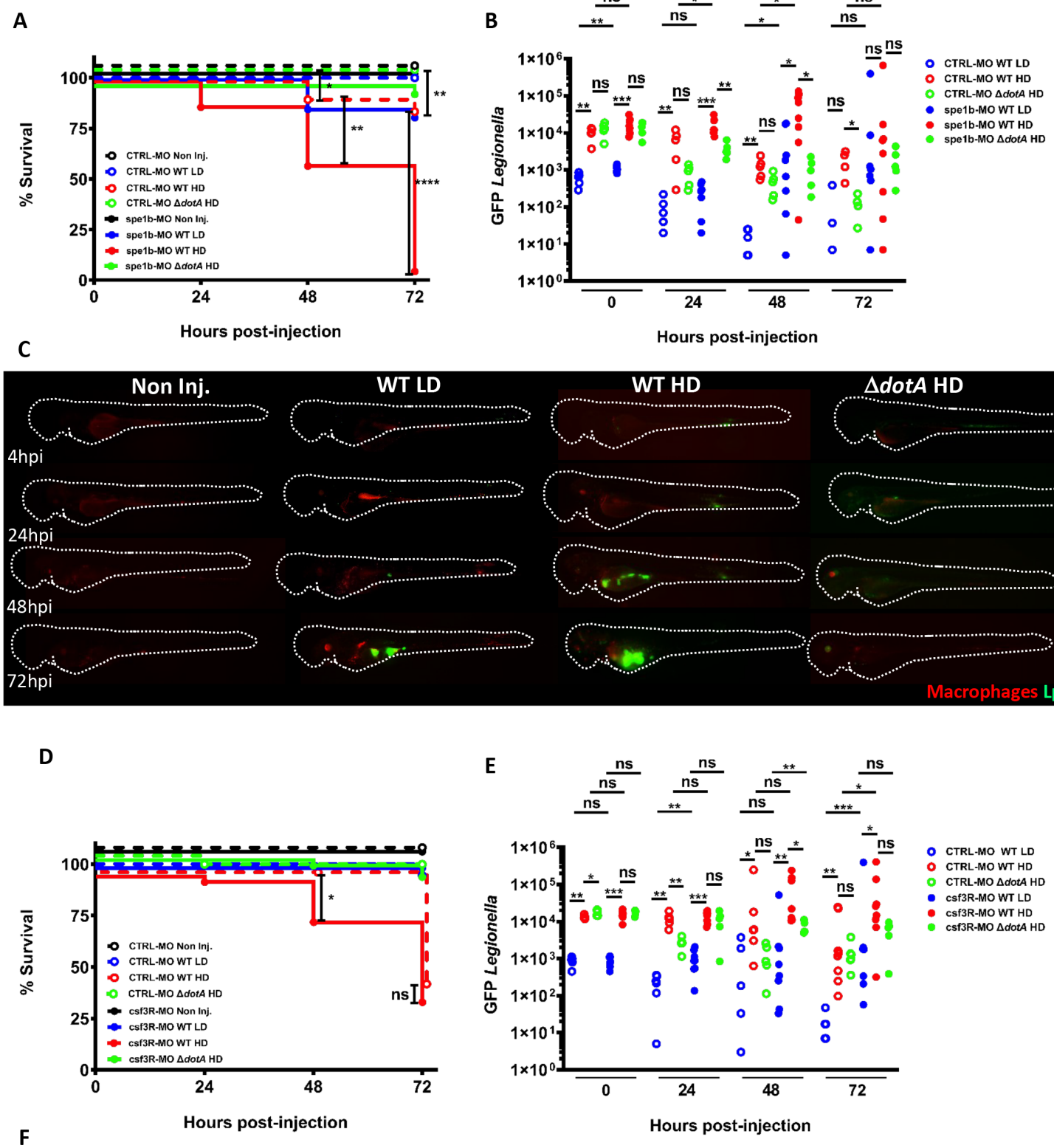
A
% Survival
Hours post-injection
CTRL-MO Non Inj.
CTRL-MO WT LD
CTRL-MO WT HD
CTRL-MO ΔdotA HD
spe1b-MO Non Inj.
spe1b-MO WT LD
spe1b-MO WT HD
spe1b-MO ΔdotA HD
B
GFP Legionella
Hours post-injection
C
Non Inj.
WT LD
WT HD
ΔdotA HD
4hpi
24hpi
48hpi
72hpi
Macrophages Lpp
D
% Survival
Hours post-injection
csf3R-MO Non Inj.
csf3R-MO WT LD
csf3R-MO WT HD
csf3R-MO ΔdotA HD
E
GFP Legionella
Hours post-injection
F
Non Inj.
WT LD
WT HD
ΔdotA HD
4hpi
24hpi
48hpi
72hpi
Neutrophils Lpp

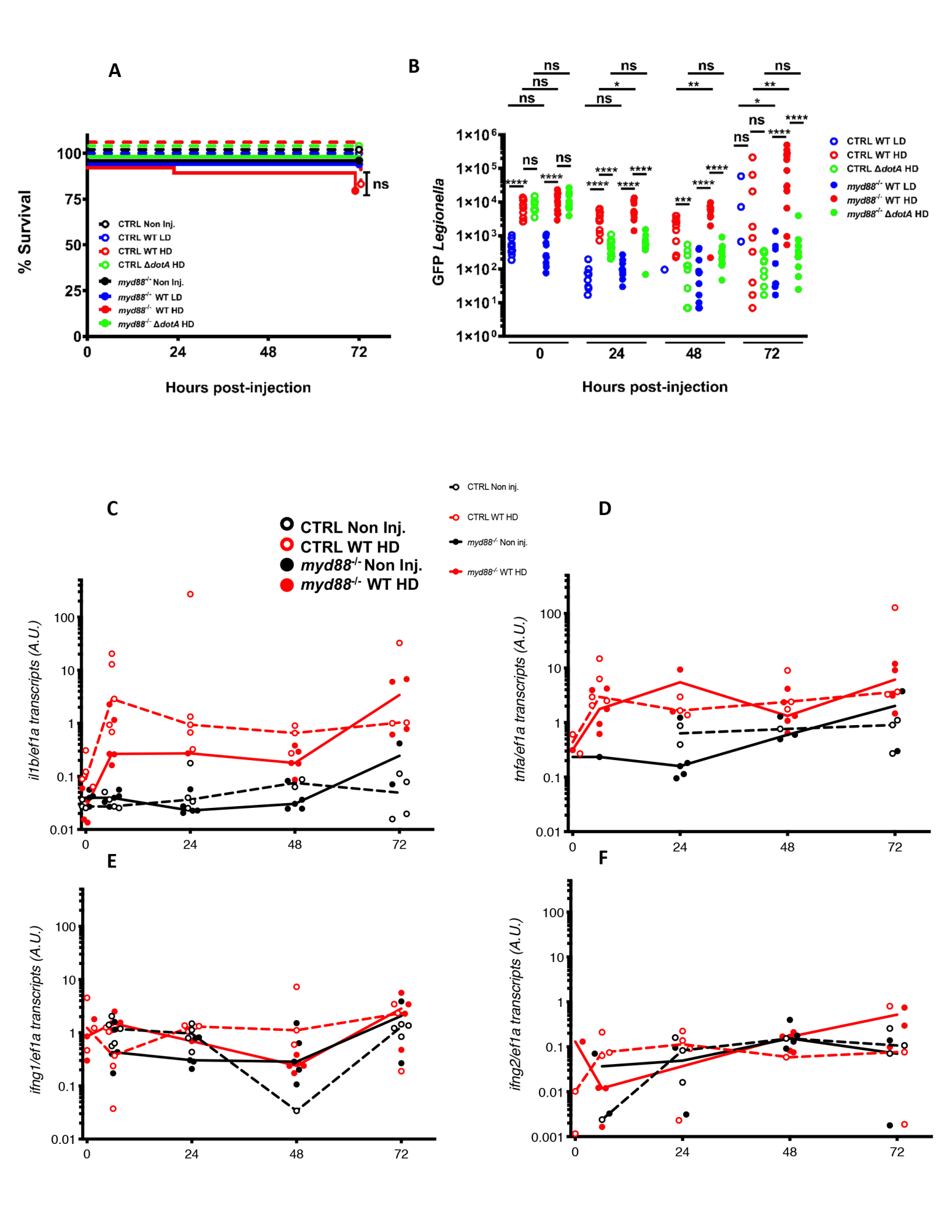
A
% Survival
100
75
50
25
0
ns
CTRL Non Inj.
CTRL WT LD
CTRL WT HD
CTRL ΔdotA HD
myd88-/- Non Inj.
myd88-/- WT LD
myd88-/- WT HD
myd88-/- ΔdotA HD
0
24
48
72
Hours post-injection
B
GFP Legionella
1×10^6
1×10^5
1×10^4
1×10^3
1×10^2
1×10^1
1×10^0
ns
*
**
***
****
CTRL WT LD
CTRL WT HD
CTRL ΔdotA HD
myd88-/- WT LD
myd88-/- WT HD
myd88-/- ΔdotA HD
0
24
48
72
Hours post-injection
C
CTRL Non Inj.
CTRL WT HD
myd88-/- Non Inj.
myd88-/- WT HD
il1b/ef1a transcripts (A.U.)
100
10
1
0.1
0.01
0
24
48
72
D
CTRL Non inj.
CTRL WT HD
myd88-/- Non inj.
myd88-/- WT HD
tnfa/ef1a transcripts (A.U.)
100
10
1
0.1
0.01
0
24
48
72
E
ifng1/ef1a transcripts (A.U.)
100
10
1
0.1
0.01
0
24
48
72
F
ifng2/ef1a transcripts (A.U.)
100
10
1
0.1
0.01
0.001
0
24
48
72

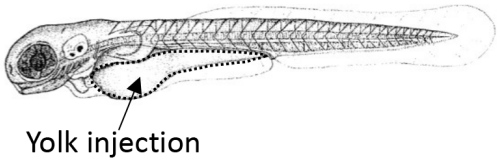
Yolk injection

A

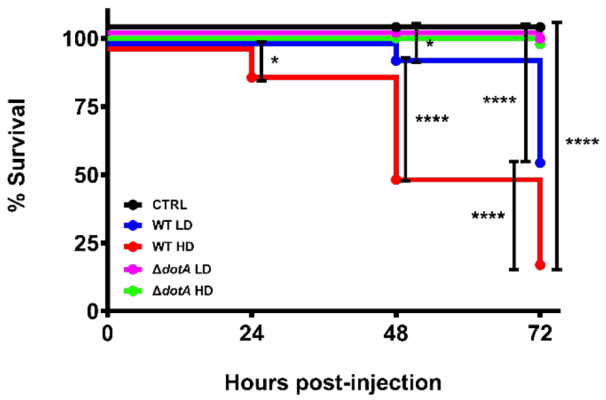
% Survival
100
75
50
25
0
0
24
48
72
Hours post-injection
CTRL
WT LD
WT HD
ΔdotA LD
ΔdotA HD
*
*
****
****
****
****

B

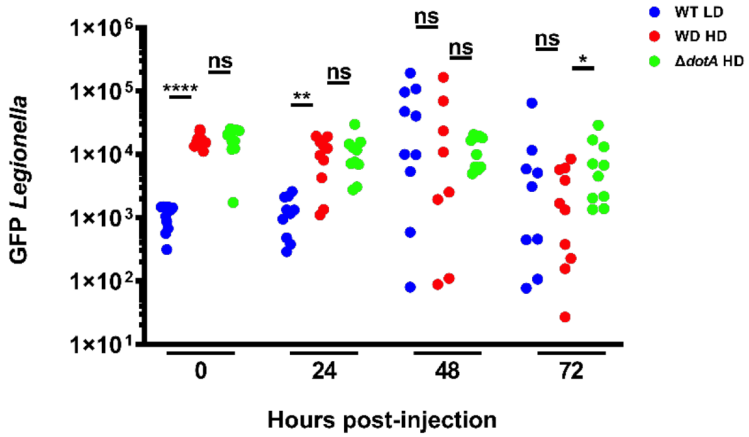
GFP Legionella
1×10⁶
1×10⁵
1×10⁴
1×10³
1×10²
1×10¹
0
24
48
72
Hours post-injection
WT LD
WD HD
ΔdotA HD
****
ns
**
ns
ns
ns
ns
*

C

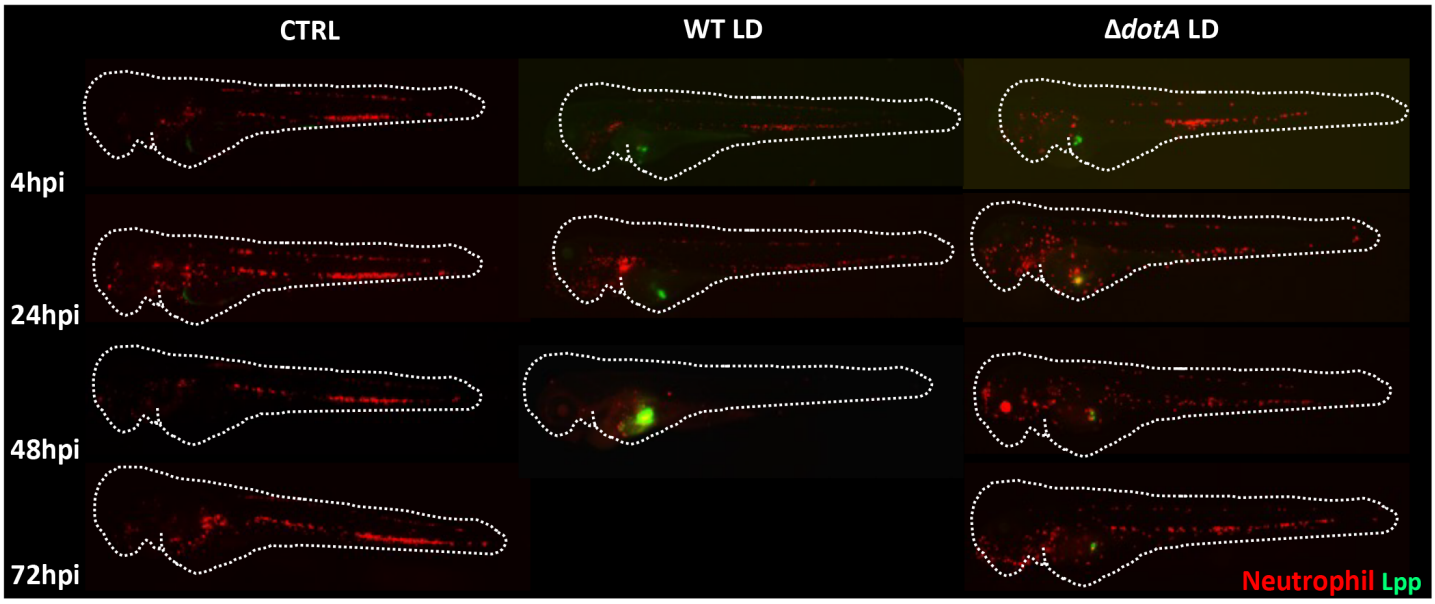
CTRL
WT LD
ΔdotA LD
4hpi
24hpi
48hpi
72hpi
Neutrophil Lpp

D

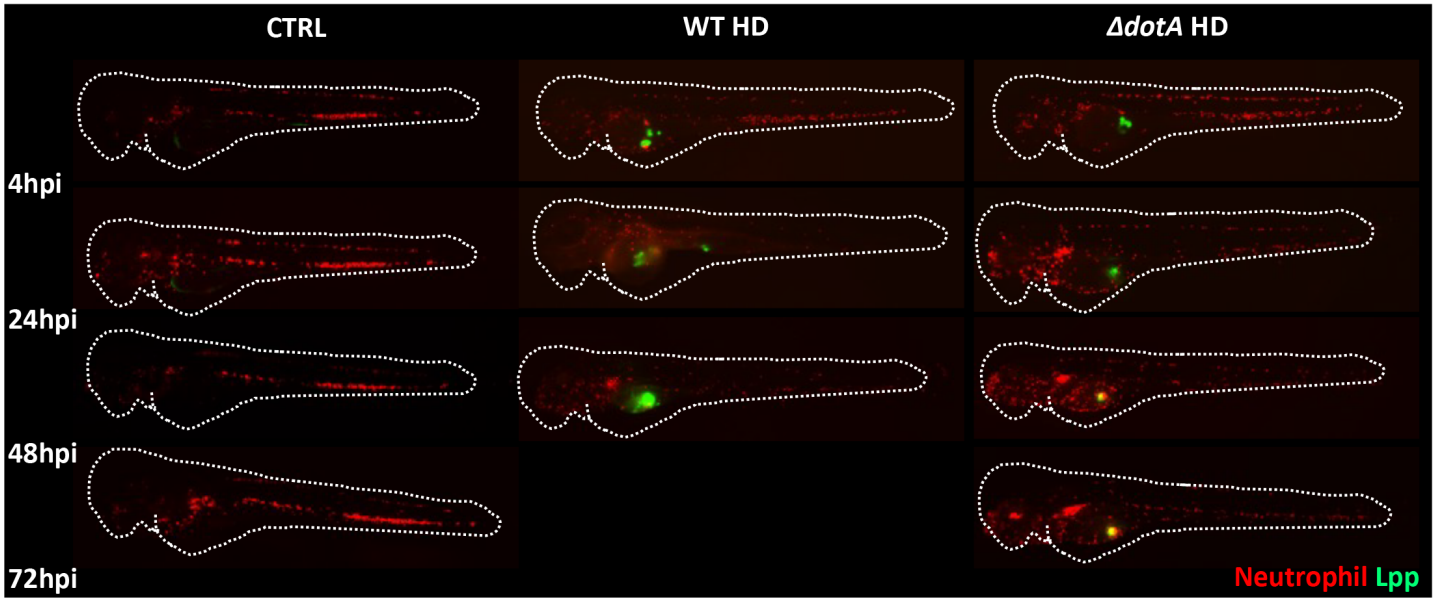
CTRL
WT HD
ΔdotA HD
4hpi
24hpi
48hpi
72hpi
Neutrophil Lpp